Wang *et al. Cell & Bioscience* (2025) 15:170
https://doi.org/10.1186/s13578-025-01513-8

Cell & Bioscience

RESEARCH Open Access

Deciphering the epigenomic regulatory variations reveals function diversity in adipose lineage among different adipose depots of pigs

Daoyuan Wang[1,3†], Renzhuo Kuang[1†], Mingyang Hu[3†], Jiahao Sun[1], Zhixiang Xu[1], Yu Shen[1], Hao Peng[1], Xiaolong Qi[3], Honghong Zhou[3], Yaping Guo[1], Ruixian Ma[1], Zheyu Han[1], Yan Zhang[1], Yixin Zhao[3], Mengjin Zhu[1,2*], Yinlong Liao[3*] and Yunxia Zhao[1,3*]

Abstract

The distribution of adipose depots in different body parts affects pig production value and human health, governed by complex epigenomic mechanisms. Limited studies on pig adipose depots have hindered the genetic improvement of fat-related economic traits and their biomedical applications. To address this issue, we generated epigenomic maps for backfat, belly fat, groin fat, and intermuscular fat (IMF) in Meishan pigs, integrating ChIP-seq, ATAC-seq, RNA-seq, Hi–C, and public whole-genome sequencing data. Our results reveal that belly/backfat share similar chromatin states, while groin fat/IMF exhibit distinct H3K27ac modification, super-enhancer (SE) dynamics, and open chromatin landscapes compared to belly/backfat. The spatially specific expressions of adipogenic transcription factors (TFs), such as lipid synthesis-related TFs PPARA and SOX6, which are highly expressed in back/belly fat, and adipocyte differentiation TF KLF4 was driven by a groin fat specific SE, underlie these chromatin state disparities. These results also suggest enhanced lipid synthesis in belly/backfat and adipocyte differentiation in groin fat. Moreover, candidate functional variants identified in IMF-gained H3K27ac peaks are primarily associated with meat quality traits. Genes linked to pig backfat thickness may also serve as candidate genes for human obesity due to the conserved *cis*-regulatory elements and gene expression patterns between humans and pigs. Overall, our epigenomic landscape enhances understanding of adipose depot regulation in mammals, facilitating cross-species insights and precision breeding.

Keywords Different adipose depots, *Cis*-regulatory elements, Backfat thickness, IMF content, Functional variants

†Daoyuan Wang, Renzhuo Kuang and Mingyang Hu have contributed equally to this work.

*Correspondence:
Mengjin Zhu
zhumengjin@mail.hzau.edu.cn
Yinlong Liao
liaoyinlong@yzwlab.cn
Yunxia Zhao
yxzhao@mail.hzau.edu.cn
[1]Key Laboratory of Agricultural Animal Genetics, Breeding, and Reproduction of the Ministry of Education and Key Laboratory of Swine Genetics and Breeding of Ministry of Agriculture, Huazhong Agricultural University, Wuhan, China
[2]The Cooperative Innovation Center for Sustainable Pig Production, Wuhan, China
[3]Yazhouwan National Laboratory, Sanya City, China

Introduction

In mammals, adipose tissue is pivotal in energy storage and provision. Moreover, it is distributed across various body regions and exerts multiple biological functions as a secretory organ. For example, mesenteric adipose tissue responds to inflammatory bowel disease [1], adipocytes in mammary glands and the heart supply lipids to adjacent cells for nutrition [2], and visceral fat is closely associated with health issues such as heart disease, hypertension, and diabetes [3, 4]. In pigs, recent studies reveal that adipose tissue contributes to adaptation under cold stress through modulation of immune function [5]. Beyond its physiological roles, adipose tissue also plays a crucial role in determining the economic value of livestock such as pigs, where fat deposition is directly related to pork quality. For example, intramuscular fat content influences the taste and flavor of pork [6], while reducing backfat thickness is commonly used as a standard for maximizing lean meat yield [7]. Moreover, fat deposition is correlated with growth rate and weight gain. In breeding programs, selecting pigs with high-quality meat that meets market demands requires considering the distribution and levels of fat to ensure optimal meat quality and production yield.

Pigs boast the highest adiposity among meat-producing animals, making them an ideal model for investigating adipose tissue metabolism and associated pathologies in humans [3]. Native Chinese pig breeds are known for their adaptability to environments, disease resistance, and unique genetic traits. Specifically, Chinese Meishan (MS) pigs exhibit a higher intermuscular fat (IMF) content, superior meat quality, and thicker backfat compared to western commercial pigs such as the Large White (LW) pigs [8]. Compared with traditional rodent models, pigs (Sus scrofa) share greater similarity with humans in anatomical size and structure, physiology, immunology, and genome organization, which enhances their translational value [9]. Importantly, pigs and humans both exhibit distinct regional partitioning of fat depots, such as subcutaneous adipose tissue (SAT) and visceral adipose tissue (VAT), with comparable distribution patterns and metabolic characteristics [10, 11]. Moreover, conserved transcriptional regulation has been observed for key adipogenic transcription factors (e.g., CEBPB51 and PPARG23) and inflammatory signal factor IL6ST in humans and pigs [12]. These parallels underscore the suitability of pigs as a physiologically relevant model for studying human adipose metabolism, obesity, and related metabolic diseases. Therefore, exploring the mechanisms of fat deposition and metabolism in different adipose depots of pigs is of great importance for understanding human fat-related diseases, particularly obesity, and improving the economic benefits of the pig industry.

An increasing body of research has underscored the critical role of the three-dimensional (3D) architecture of the mammalian genome in regulating gene transcription [13, 14]. Previous studies have demonstrated how dietary interventions reshape topologically associating domain (TAD) structures and transcriptional patterns in porcine subcutaneous and visceral adipose depots through pig models of diet-induced weight gain and weight loss [12]. Nevertheless, chromatin conformation capture techniques based on chromatin interactions have limited resolution [15], and therefore incorporating information about *cis*-regulatory elements and chromatin state is required to offer a more detailed landscape for gene expression regulation. However, knowledge of the *cis*-regulatory elements and their regulation functions in different adipose depots of pigs remains poorly understood.

Here, to construct a more reliable and comprehensive gene expression regulatory landscapes of pig adipose depots, we conducted chromatin immunoprecipitation sequencing (ChIP-seq) for histone H3 lysine 27 acetylation (H3K27ac), assay for transposase-accessible chromatin with sequencing (ATAC-seq), transcriptome profiling (RNA-seq) across four adipose depots (backfat, belly fat, groin fat and IMF), as well as Hi-C sequencing for backfat and groin fat, in adult MS pigs. Integrative analysis of these datasets enabled systematic annotation of *cis*-regulatory elements and transcriptional landscapes, candidate functional mutation sites, and conservation of *cis*-regulatory elements between pig and human. Moreover, we confirmed the regulatory activity of identified *cis*-regulatory elements via dual-luciferase reporter assays, while knockdown of depot-specific TFs validated their context-dependent roles in different adipose depots. Together, these findings offer critical insights into the regulatory landscape of porcine adipose depots, with potential implications for improving meat quality and advancing our understanding of the pathogenesis of human adipose-associated traits.

Results

Overview of cis-regulatory elements in four pig adipose depots

In this study, we generated H3K27ac ChIP-seq, ATAC-seq, and RNA-seq libraries from four adipose depots (backfat, belly fat, groin fat, and IMF) of adult MS pigs (Fig. 1A). Multidimensional scaling (MDS) analysis of each data type revealed clear separation among depot types, with replicates clustering tightly together (Fig. S1A–C). On average, we obtained approximately 39 million reads per H3K27ac ChIP-seq library, 156 million reads per ATAC-seq library, 38 million reads per RNA-seq library (Supplementary Tables 1, 2 and 3). In addition, we generated Hi-C 3.0 libraries for backfat and groin fat, with an average of 663 million reads per

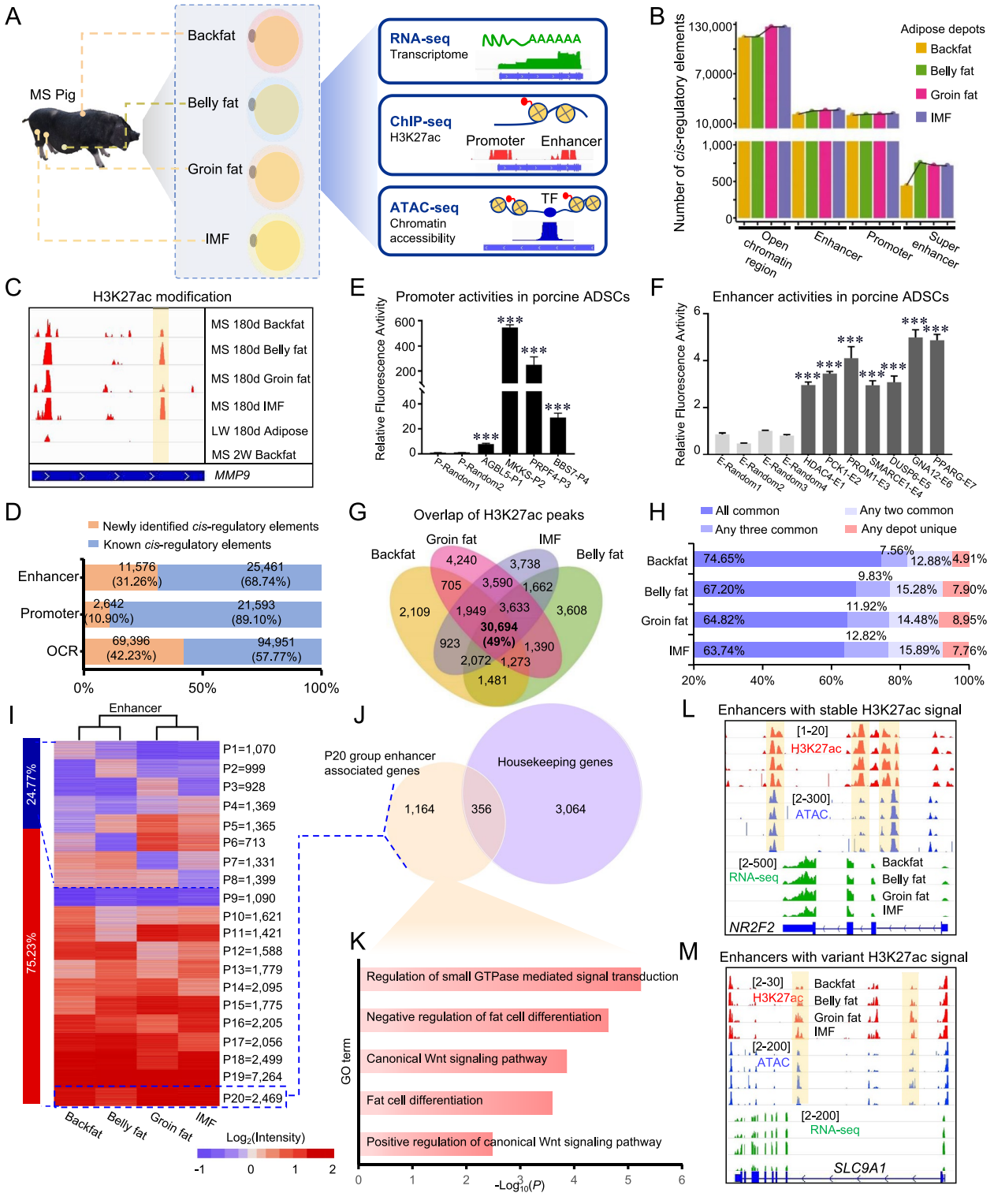

Fig. 1 (See legend on next page.)

sample (Supplementary Table 4). For RNA-seq, ChIP-seq, and ATAC-seq data, more than 89.20% of the RNA-seq mapped reads aligned uniquely to the pig reference genome (susScr11), while over 68.87% and 72.15% of the total mapped reads of ChIP-seq and ATAC-seq libraries were in the deduplicated BAM files, respectively (Supplementary Tables 1, 2 and 3). The Pearson correlation coefficients (PCCs) between replicates exceeded 0.9 for

(See figure on previous page.)

Fig. 1 Identification and comparison of *cis*-regulatory elements across fat depots. **A** Schematic of experimental design. **B** Summary of *cis*-regulatory elements identified in four adipose depots. **C** Genome browser views of the *MMP9* gene showing H3K27ac ChIP-seq signals from published data and this study. **D** Statistical analysis of newly identified *cis*-regulatory elements for adipose tissues in this study. The published backfat data (blue) of four pig breeds (MS, ES, LW, and Duroc) at two weeks of age and adult LW pigs from FAANG project were used for comparing. **E**–**F** Verification of promoter and enhancer activities using dual-fluorescence reporter system in porcine ADSCs. P/E-random were negative controls. The *P*-value was calculated using Student's t-test, and the data are mean ± standard deviation (n = 4), with *** indicating $P < 0.001$. **G** Venn diagram showing the overlapping of H3K27ac peaks across four adipose depots. **H** Percentages of H3K27ac ChIP-seq peaks in each fat depot that are common to all, any three, any two, or only one depot, respectively. (**I**) Heatmap of H3K27ac intensity patterns for enhancers from four adipose depots (parameters of K-means with centers = 20, iter.max = 40). The 24.77% (in blue) and 75.23% (in red) of enhancers showed differential and stable H3K27ac modification across the four adipose depots, respectively. **J** Venn diagram showing the overlap between genes associated with P20 enhancers cluster and housekeeping genes. (K) Bar plot of enriched GO terms for P20-related genes excluding non-housekeeping genes. (L-M) Examples of genome browser screenshots showing the regions around the *NR2F2* and *SLC9A1* genes.

each data type (Supplementary Tables 1, 2 and 3). The normalized strand coefficients (NSC, > 1.05) and relative strand correlation (RSC) values (> 0.8) for the H3K27ac ChIP-seq data and ATAC-seq data, TSS enrichment values (> 5) for the ATAC-seq data, and the fraction of reads in peak (FriP) values (> 0.2) for ChIP-seq data all surpassed the ENCODE-established thresholds, confirming that both the ChIP-seq and ATAC-seq datasets were of high quality (Supplementary Tables 2 and 3). For Hi-C 3.0 data, 36–40% unique reads were in Hi-C contacts, cis/trans interactions were 3.52–3.64, and unique reads in long range contacts (> 20 kb) were 54.46–69.42% (Supplementary Table 4). These results confirm the robustness of our dataset and its suitability for downstream integrative analysis.

The quality-controlled datasets were utilized to identify cis-regulatory elements following the ENCODE guidelines (https://www.encodeproject.org/). In total, 21,044–26,298 active enhancers, 20,072–21,857 active promoters, 444–761 super-enhancers (SEs), and 114,061–126,892 open chromatin regions were identified across the four adipose depots (Fig. 1B, Supplementary Table 5). Our study newly identified *cis*-regulatory elements that were not observed in the previous studies, such as an active enhancer within *MMP9*, which was identified in our adult MS pig adipose tissue but was absent in prior surveys of adult LW pig and MS 2W backfat [11, 16] (Fig. 1C). Comparative analysis uncovered that 31.26% of active enhancers, 10.90% of active promoters, and 42.23% of open chromatin regions in adipose depots were newly identified in this study (Fig. 1D, S1D & E). We further performed dual-luciferase reporter assays on four randomly selected promoter regions and seven enhancer regions in porcine backfat ADSCs (adipose-derived stem cells) and PK-15 cells. All tested elements showed significantly higher luciferase activity than genomic barren region, supporting the reliability of our *cis*-regulatory elements identification (Figs. 1E & F, S1F & G). Together, these results demonstrate although recent efforts have substantially advanced *cis*-regulatory elements annotation in the pig genome, depot-specific profiling remains essential for refining and expanding the regulatory landscape.

Next, across the four adipose depots, we identified 30,694 common H3K27ac peaks (nearly 50% of total H3K27ac peaks), which were consistently shared across all depots and constituted 60–70% of the H3K27ac peaks in each adipose depot (Fig. 1G & H). A parallel analysis of ATAC-seq data revealed a comparable pattern of shared open chromatin regions (Fig. S1H & I). K-means clustering revealed that the P20 groups of stable enhancers and promoters exhibited the strongest H3K27ac signals across adipose depots, corresponding to 1520 and 1497 genes, respectively. Among these genes 76.57–84.04% of which were non-housekeeping genes in pigs (Figs. 1I & J, S2A & B). GO analysis of above non-housekeeping genes indicated that these common *cis*-regulatory elements indeed play adipose depots-related functions (e.g., fat cell differentiation for enhancers and Wnt signaling pathway for promoters) (Figs. 1K & S2C). As examples, we indeed observed consistent stable H3K27ac and ATAC-seq signals across the four adipose depots in stable expressed adipocyte differentiation gene *NR2F2* promoter [17] and *ID4* enhancers [18] (Figs. 1L & S2D). In addition, almost a quarter (24.77%) of enhancers and 21.73% of promoters exhibited differences in H3K27ac modification across the four adipose depots (Figs. 1I & S2A). For instance, the pro-lipogenic gene *SLC9A1* [19] and the matrix metallopeptidase gene *MMP27* [20] showed higher expression in groin fat than in other depots, correlating with higher H3K27ac and ATAC-seq signals in the respective enhancers or promoters in groin fat (Figs. 1M & S2E). These results highlight both shared and depot-specific transcriptional regulatory patterns among adipose depots in pigs.

The most significant differences in chromatin states between belly fat and groin fat, as well as IMF, leading to variations in lipid synthesis capacity

To further dissect the regulatory divergence in gene expression across the four adipose depots in detail, we performed differential analysis of H3K27ac peak densities in promoters and enhancers regions using edgeR (refer to Methods). In each comparison, over 74% of the differential H3K27ac peaks were located in enhancer

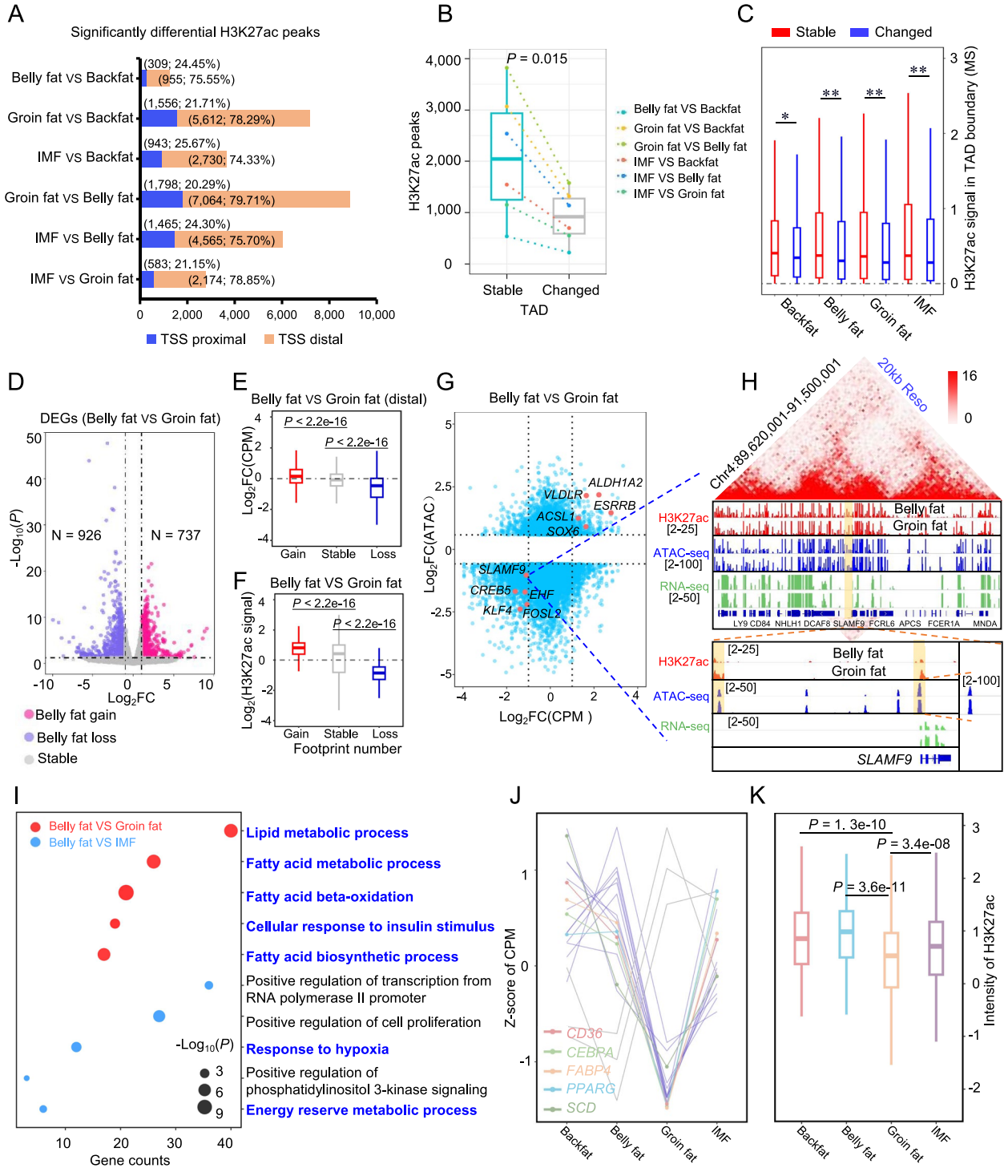

Fig. 2 (See legend on next page.)

regions (TSS distal regions), and approximately a quarter were located around the TSS (Fig. 2A). Moreover, it is worth noting that the least variation in H3K27ac signals was observed between backfat and belly fat, indicating that these two adipose depots share the highest similarity in gene expression regulation and biological function. The most considerable variation in H3K27ac signal was observed between belly fat (or backfat) and groin fat, as well as between belly fat and IMF (Fig. 2A).

TADs were broadly reported to represent a fundamental layer of 3D genome organization with remarkable stability across tissues, developmental stages, and

(See figure on previous page.)

Fig. 2 Integrated analysis of differences in histone modification, gene expression and chromatin accessibility between belly fat and groin fat. **A***Cis*-regulatory elements with significant differences in H3K27ac modification among four adipose depots. TSS proximal/distal represent promoter/enhancer regions, respectively. **B** Distribution of variable H3K27ac signal peaks in stable and changed TADs identified using backfat and groin fat from MS pigs. **C** Enrichment of the H3K27ac modification intensity for each adipose depots at boundaries of stable and changed TADs identified using backfat and groin fat from MS pigs. **D** Volcano plot showing genes differentially expressed between belly fat and groin fat. **E** Boxplot indicating the fold change (FC) in gene expression following differential histone modification of enhancers inside stable TADs between belly fat and groin fat. Gain, stable and loss indicate changes of H3K27ac signal intensity in enhancers. **F** Boxplots indicating the FC in H3K27ac signal densities in *cis*-regulatory elements following changes of footprint number inside stable TADs between belly fat and groin fat. Gain, stable and loss indicate changes in footprint number. **G** Scatter plot showing the gene expression levels and open chromatin state between belly fat and groin fat. **H** Genome browser screenshots indicating the changes of H3K27ac ChIP-seq and ATAC-seq signals at the promoter and enhancer regions of the *SLAMF9* gene, as well as the expression levels, between belly fat and groin fat. The Hi-C heatmap is derived from UBL of Bama pigs. The *P*-values in **B**, **C**, **E** and **F** were calculated using a single-sided unpaired Wilcoxon test. * indicates $P < 0.05$, ** indicates $P < 0.01$. (I) GO enrichment analysis of DEGs between belly fat and groin fat, and between belly fat and IMF. **J** Z-score for expression levels of 19 lipid synthesis-promoting genes across four adipose depots. Only five classic lipid synthesis-promoting genes are listed here. **K** Boxplot showing H3K27ac intensity in enhancers of lipid synthesis-promoting genes differentially expressed across the four adipose depots inside stable TADs of Bama pigs. The *P*-values were calculated using a single-sided paired Wilcoxon test.

even species [21, 22]. A previous study demonstrated that TADs changed between the upper layer of backfat (ULB) and greater omentum fat (GOM, which is similar to groin fat [3]) of Bama pigs, and these alterations were correlated with differences in gene expression [23]. Using the Hi-C data from backfat and groin fat, we identified TADs and found that approximately 80% of TADs were conserved between the two adipose tissues (Fig. S3A), and the variable H3K27ac modification signal were significantly located within the stable TADs than these located within the changed TADs (Figs. 2B & S3C). Furthermore, when compared with changed TADs, stronger H3K27ac and ATAC-seq signals were observed at the boundaries of stable TADs across all four adipose depots (Figs. 2C & S3F). We further identified ULB and GOM TADs in Bama pig using published data [23] (Fig. S3B). Interestingly, we found similar H3K27ac and ATAC signal features in both Bama and Meishan pigs (Fig. S3D-E and G-H). These findings reinforce the notion that TADs, as fundamental structural units of the genome, are highly conserved across pig breeds in the same tissue types. Together, our results suggest that depot-specific transcriptional differences may largely be driven by enhancer-promoter interactions within stable TADs, rather than by large-scale changes in TAD organization.

Based on the results showing that belly fat and groin fat, as well as belly fat and IMF, exhibit the most significant disparities in H3K27ac signals (Fig. 2A), we further investigated the relationship between gene expression and variations in H3K27ac or ATAC-seq signals inside stable TADs across these adipose depots. There were 1,663 differentially expressed genes (DEGs) ($|\log_2 FC| > 1$ and $P < 0.05$) between belly fat and groin fat, and 843 DEGs between belly fat and IMF (Figs. 2D & S3I). Further statistical analysis confirmed that within stable TADs, H3K27ac level changes at enhancers/promoters correlated with corresponding gene expression changes (Figs. 2E & S3J-L). Moreover, changes in TF binding (i.e., changes in the number of TF footprints) at open chromatin regions captured by ATAC-seq were concordant with the changes in the H3K27ac intensities of *cis*-regulatory elements inside stable TADs (Figs. 2F & S3M). For instance, the *SLMAF9* gene, which plays a vital role in immune regulation and inflammation [24], was upregulated in groin fat, and its enhancer and promoter exhibited higher enrichment of H3K27ac and ATAC signals in groin fat compared to belly fat (Fig. 2G & H).

Next, the GO enrichment analysis showed that these DEGs were significantly enriched in pathways related to adipose tissue functions, such as lipid metabolic process, fatty acid metabolic process, and response to hypoxia (Fig. 2I). The above GO terms involved 19 known lipid synthesis-promoting genes, such as the adipogenic marker genes *SCD* [25], *PPARG* [26], and *FABP4* [27], which showed the highest expression levels in backfat and belly fat, and the lowest expression levels in groin fat (Fig. 2J). Moreover, inside the stable TAD regions, the H3K27ac and ATAC-seq signals in *cis*-regulatory elements of these lipid synthesis genes in backfat and belly fat were also significantly higher than those in groin fat (Figs. 2K & S3N). These results indicated that back and belly fat exhibit the most active lipid biosynthesis and accumulation, followed by IMF, with groin fat showing the lowest activity.

SEs typically comprise multiple typical enhancers (TEs) and are major drivers of the transcriptional activation of cell identity genes [28]. We then explored the regulation of SEs in the four adipose depots. As expected, in each adipose depot, the SE-associated genes showed significantly higher expression levels than TE-associated genes (Fig. 3A-D). GO enrichment analysis showed that the SE-associated genes in the four adipose depots play key biological functions of adipocytes (Fig. 3E). Notably, we observed the long-chain fatty acid transport is enriched only in backfat and belly fat, and the white fat cell differentiation is only enriched in groin fat (Fig. 3E). These results indicated that SEs regulated important biological functions of adipose tissues, and were dynamic across different adipose depots, which may account for depot-specific biological functions variation.

To further characterize the functions and features of SEs in transcriptional regulation in each adipose depot, we systematically investigated the dynamic changes of SEs. Sankey plot uncovered dramatic SEs dynamic regulation across the four adipose depots (Fig. 3F), and totally 349 (44.98%) SEs switched to TEs among adipose depots (Fig. 3G). As for these dynamic SEs, groin fat exhibited the highest number (Fig. 3H). Notably, depot-specific SE-regulated genes in belly fat and backfat exhibited significant enrichment in biological pathways related to long-chain fatty acid transport and lipid metabolic processes (Fig. S4), including lipid synthesis-promoting genes such as *CD36* [29], *FABP4* [27], and *FABP5* [30]. These genes indeed have higher expression levels in belly fat and backfat (Fig. 3I & J). Depot-specific SE associated genes in groin fat exhibited significant enrichment in functional pathways related to RNA polymerase II-mediated transcription and cell differentiation processes, including adipocyte differentiation-promoting genes such as *KLF4* [31], *ID2* [32], and *LGMN* [33], and these genes were highly expressed in groin fat (Fig. 3I & K). Together, these findings further corroborate the elevated lipid synthesis and fat deposition observed in backfat and belly fat (Fig. 2J), and additionally indicate enhanced adipogenic differentiation in groin fat.

Spatially specific expressions of adipogenic transcription factors drive the differential activities of cis-regulatory elements across adipose depots

The spatially specific expression of transcription factors (TFs) and their binding to *cis*-regulatory elements are critical for transcriptional regulation in cells. To identify TFs contributing to adipose depot-specific differences, we analyzed the TF binding motifs enriched in ATAC-seq footprints of *cis*-regulatory elements. In the comparison between belly fat and groin fat, 26 motifs were uniquely enriched in ATAC-seq footprints of *cis*-regulatory elements with both upregulated H3K27ac and ATAC-seq signals in belly fat (Figs. 4A & S5A), which included more belly fat upregulated TFs (5 up-regulated TFs vs. 2 down-regulated TFs) (Fig. 4B & C). These five significantly upregulated TFs in belly fat were ESSRB, SOX6, ETV2, PGR, and PPARA (Fig. 4A & C). Meanwhile, 33 motifs were uniquely enriched in ATAC-seq footprints of *cis*-regulatory elements with both H3K27ac and ATAC-seq signals upregulated in groin fat (lost in belly fat) (Fig. S5A), and it only included five groin fat upregulated (belly fat downregulated) TFs, namely HOXD13, FOXM1, RFX2, FOSL2, and KLF4 (Fig. 4D & E). Notably, transcription factors ESRRB, SOX6, PGR, and PPARA have been implicated in promoting lipid synthesis and fat deposition [34–37]. While transcription factors FOSL2 and KLF4 are known to enhance adipocyte differentiation [31, 38]. This further strengthens our conclusion that belly fat has a stronger ability to lipid synthesis and fat deposition, while groin fat is more prone to adipogenic differentiation.

When comparing belly fat and IMF, 24 motifs were uniquely enriched in ATAC-seq footprints of *cis*-regulatory elements with both H3K27ac and ATAC-seq signals upregulated in belly fat (Fig. S5B-C). In these 24 uniquely enriched motifs, two upregulated TFs (SPDEF and PGR) and only one down-regulated TF (KLF5) were observed in belly fat (Fig. S5D & E). Moreover, 34 motifs were uniquely enriched in ATAC-seq footprints of *cis*-regulatory elements with both H3K27ac and ATAC-seq signals upregulated in IMF (loss in belly fat) (Fig. S5B & C). Among these, three TFs upregulated in IMF (HOXD13, HOXA10, and HOXA13) and only one upregulated in belly fat (PITX1) were identified (Fig. S5F & G). Notably, transcription factors HOXA10 and HOXA13 have been reported to participate in muscle cell formation and regeneration [39].

In addition, we also identified 102 motifs of expressed TFs enriched in common *cis*-regulatory elements with stable H3K27ac and ATAC-seq signals across the four depots (Figs. 4F & S5H). After filling out the motifs in the footprint of differential *cis*-regulatory elements between belly fat and groin fat, and between belly fat and IMF, 29 motifs were uniquely enriched in the footprints of the common *cis*-regulatory elements (Fig. S5H), and these TFs were stably expressed across the four adipose depots (Fig. 4G). The aforementioned TFs enriched in common *cis*-regulatory elements are involved in broad, adipose-critical biological processes. Notably, ARNT (HIF-1β) and CLOCK play crucial roles in circadian metabolic regulation and obesity/body weight control [40, 41]; E2F family members and Bhlhe40 govern cell proliferation, differentiation, and apoptosis [42, 43]; while TFE3 and PBX1 participate in extensive signaling pathways and transcriptional control [44, 45].

To further validate the depot-specific expression pattern of TFs, we performed RT–qPCR across distinct adipose depots. Consistent with RNA-seq profiling, the belly fat or backfat-enriched transcription factors ESRRB, PPARA, PGR, and SOX6 showed the highest expression levels in belly fat (Fig. 4H). Similarly, groin fat-specific transcription factors FOSL2, KLF4, FOXM1, and RFX2 exhibited the highest expression levels in groin fat (Fig. S5I), while IMF-enriched transcription factors HOXA13 and HOXA10 showed high expression levels in this depot (Fig. S5J). Notably, the depot-specific expression patterns of these TFs identified in this study for MS pigs were recapitulated in DLY (Duroc × Landrace × Yorkshire) three-way crossbred pigs (Fig. S5K-L), suggesting conserved depot-specific functions of these TFs.

We further analyzed gene expression during the adipogenic differentiation of porcine backfat-derived ADSCs.

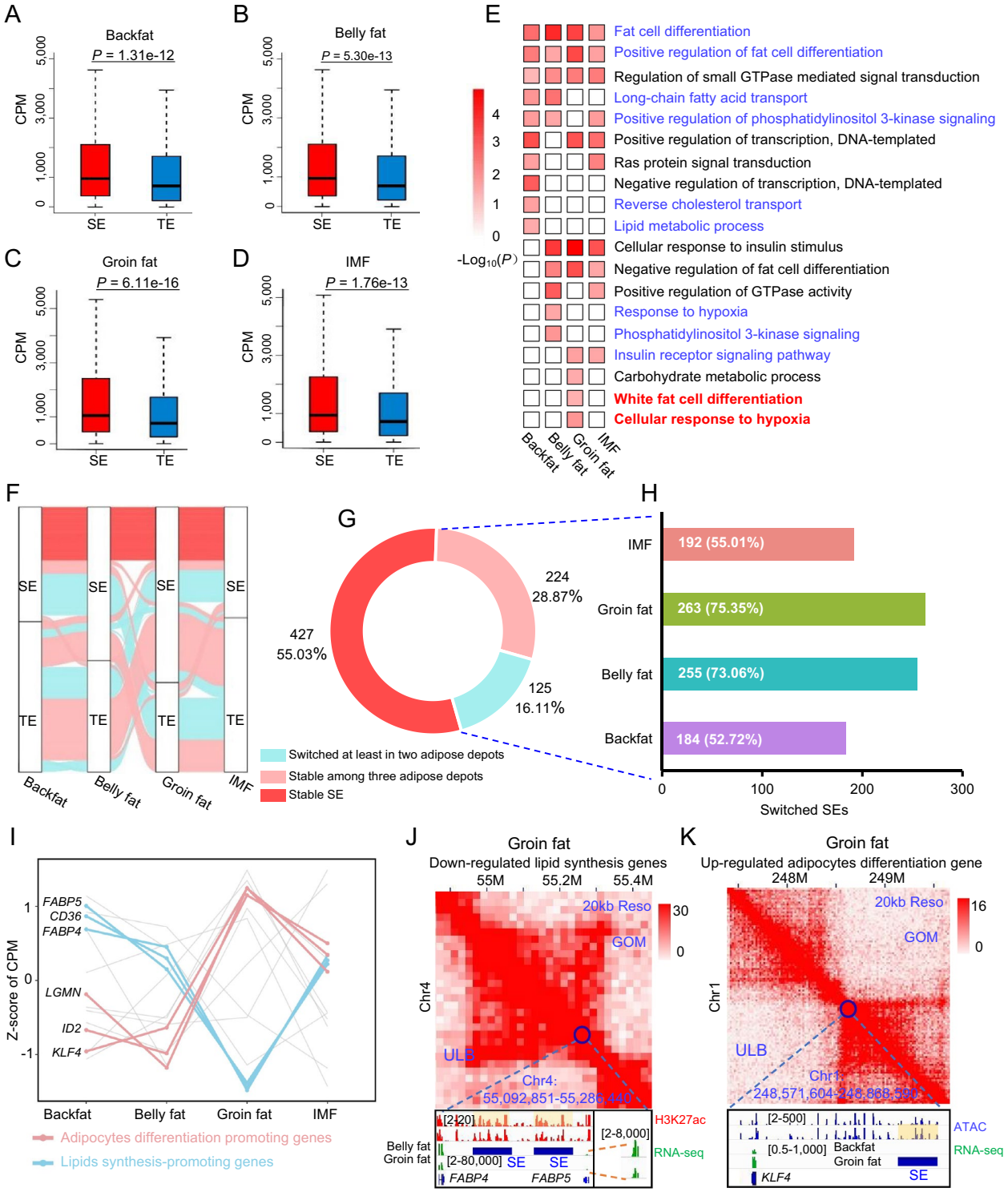

Fig. 3 Regulatory functions of SEs in different adipose depots. **A**–**D** Boxplots of the expression levels of genes regulated by SEs and TEs in backfat, belly fat, groin fat, and IMF from MS pigs. Red and blue boxes represent the CPM of genes regulated by SEs or TEs in each adipose depot, respectively. **E** Heatmap of enriched GO terms for SE-associated genes from four different adipose depots. **F** Sankey plot showing the switch between SEs and TEs across different adipose depots. **G** Overall statistics of the three types of SEs (refer to Methods). **H** Bar plot showing the number of dynamic SEs for each adipose depot. **I** Z-scores indicating the expression levels of genes regulated by SEs in groin fat that switch to TEs in belly fat and backfat (red), and genes regulated by SEs in belly fat and backfat that switch to TEs in groin fat (blue). **J** Example of genome browser screenshots illustrating the regions surrounding the down-regulated lipid synthesis genes *FABP5* and *FABP4* in groin fat, which are located in stable TADs between the ULB and the GOM. **K** Example of genome browser screenshots illustrating the regions surrounding the up-regulated adipocytes differentiation gene *KLF4* in groin fat, which is located in stable TADs between the ULB and the GOM. The *P*-values in **A**–**D** were calculated using a one-sided unpaired Wilcoxon test. *** indicates $P < 0.001$.

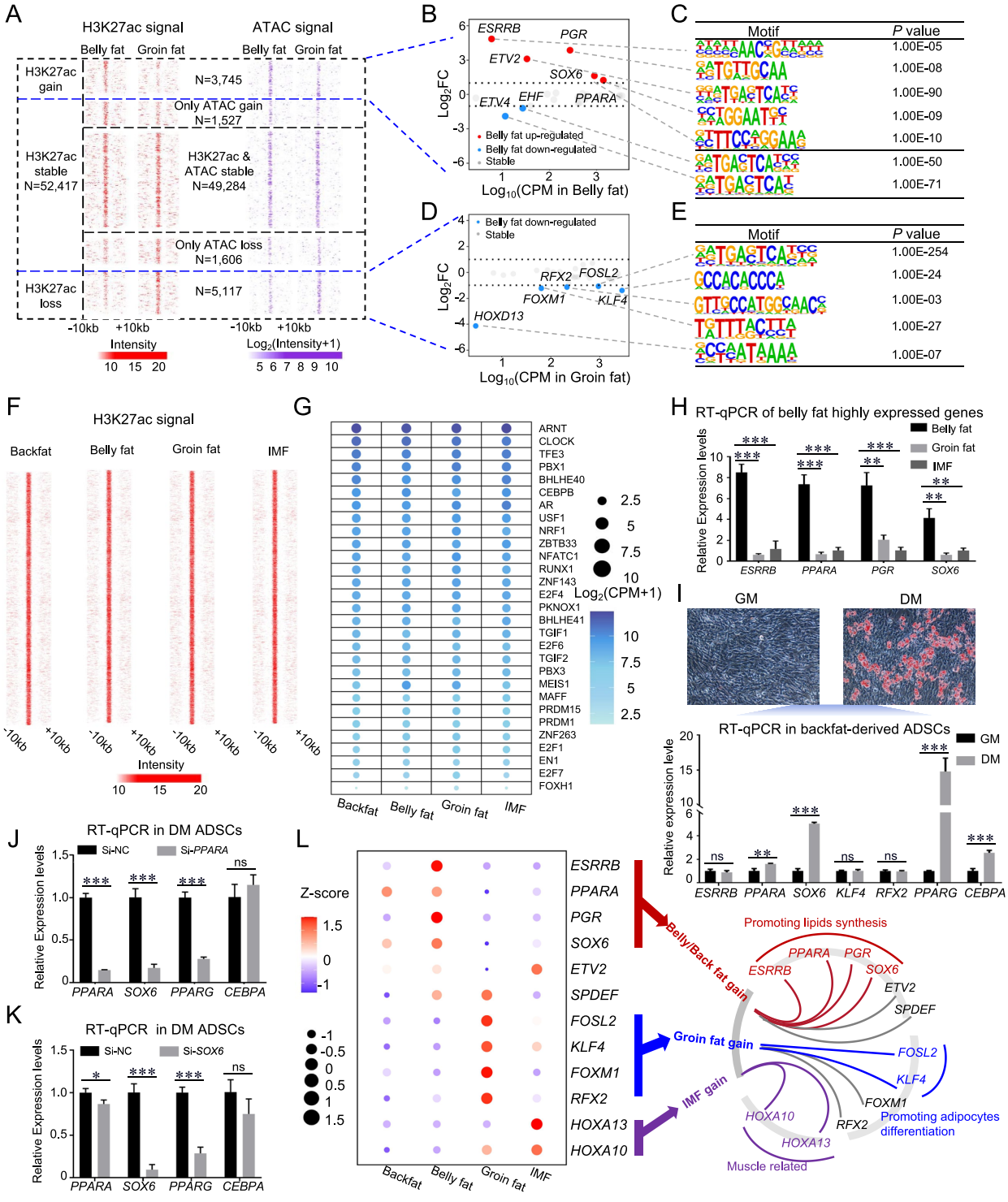

Fig. 4 (See legend on next page.)

Oil Red O staining and qPCR confirmed successful adipogenic induction, as evidenced by the upregulation of canonical markers *PPARG* and *CEBPA* (Fig. 4I). Strikingly, adipogenic induction led to robust upregulation of backfat-specific TFs (PPARA and SOX6), while belly fat-specific TF (ESRRB) and groin fat-specific TFs (KLF4 and RFX2) showed no marked changes (Fig. 4I). These findings further supporting the depots-specific expression patterns of TFs across the four adipose depots. In addition, siRNA-mediated knockdown of the backfat-specific TFs PPARA and SOX6 led to a marked reduction of the adipogenic marker gene *PPARG*, indicating a key role of

(See figure on previous page.)

Fig. 4 Enrichment of Transcription factors in adipose depots. **A** Heatmap depicting signal intensities of H3K27ac and ATAC-seq in *cis*-regulatory elements of belly fat and groin fat. "Loss, stable and gain" represent differential H3K27ac or ATAC signals in *cis*-regulatory elements between the two adipose depots. **B** Scatter plot showing differentially expressed TFs that uniquely enriched in *cis*-regulatory elements of belly fat gain. **C** Logo plots and *P* values of motifs from TFs differentially expressed between belly fat and groin fat in Fig. 4B. **D** Scatter plot showing differentially expressed TFs that uniquely enriched in *cis*-regulatory elements of belly fat loss. **E** Logo plots and *P* values of motifs from TFs differentially expressed between belly fat and groin fat in Fig. 4D. **F** Heatmap of H3K27ac intensities of common *cis*-regulatory elements across the four adipose depots. **G** Heatmap of the expression levels of the 29 TFs uniquely binding to footprints in common *cis*-regulatory elements across the four adipose depots. **H** RT-qPCR validation of belly fat high expression genes in different depots. **I** Oil Red O staining of backfat-derived ADSCs in growth medium (GM) or adipogenic differentiation medium (DM) (Top). RT-qPCR analysis showing relative expression levels of the indicated genes (Bottom). **J**-**K** RT-qPCR validation of gene expression levels after siRNA silencing treatments in adipogenic induced ADSCs. **L** Z-score of gene expressions for TFs enriched explicitly in the differentially activated *cis*-regulatory elements of different adipose depots (left), and function summaries of the adipose depots-specific upregulated TFs (right). The data presented in figures H–K are mean ± standard deviation (n = 3). The ns indicates not significant, * $P < 0.05$, ** $P < 0.01$, *** $P < 0.001$.

PPARA and SOX6 in regulating adipogenesis in porcine backfat (Fig. 4J & K). In summary, based on TFs enrichment and gene expression patterns, we identified candidate depot-specific adipocyte lineage TFs across the four distinct adipose depots in pigs (Fig. 4L & Supplementary Table 6). Specifically, TFs associated with lipid synthesis and fat deposition, including ESSRB, SOX6, PGR, and PPARA, were highly expressed in backfat (or belly fat). TFs known to promote adipocyte differentiation, such as FOSL2 and KLF4, were highly expressed in groin fat. Notably, HOXA10 and HOXA13, which are involved in myogenesis and muscle regeneration, were preferentially enriched in IMF, suggesting that IMF may exert regulatory influences on adjacent muscle cells.

Together, these analyses reveal depot-specific *cis*-regulatory elements activity, shaped by the combinatorial binding of distinct transcription factors. Belly fat is characterized by regulatory programs that favour lipid synthesis and fat deposition. whereas groin fat and intramuscular fat (IMF) are transcriptionally biased toward adipogenic commitment and muscle-related gene expression, respectively. These findings underscore the molecular diversity of adipose depots and provide mechanistic insight into their functional specialization.

Identification of candidate functional variants in adipose depot-specific cis-regulatory elements

The distribution of adipose depots in different body parts of pigs is closely associated with economic traits such as backfat thickness. Here, we collected 71 backfat thickness-associated candidate genes identified in previous pig GWAS studies (Supplementary Table 7). Among these 71 genes, 55 genes (77.46%) were expressed in all four adipose depots of this study (CPM > 1). Significantly, we found that over 58.18% (32 among 55) of the co-expression backfat thickness-associated candidate genes had similar expression patterns between backfat and IMF (Fig. 5A). These results imply that when selecting individuals with relatively thin backfat thickness during breeding, IMF content may be reduced simultaneously, which is not conducive to the improvement of meat quality traits.

As an example, the *TNFAIP8L3* gene, which plays an essential role in lipoprotein metabolism pathways [46], was a backfat thickness candidate gene identified by GWAS studies in pigs [47].We observed similar gene expression levels of this gene between IMF and backfat, accompanied by similar H3K27ac enrichment and ATAC-seq signal intensity at its promoter region in both depots (Fig. 5B). Motivated by this finding, we collected functional variants from the IFmut database (http://www.ifmutants.com:8210/#/home) and identified 1598 and 2803 candidate functional variants with a high/moderate confidence of disrupting TF binding [48] in uniquely H3K27ac gained *cis*-regulatory elements in backfat and IMF, respectively (Fig. 5C). The trait enrichment analysis confirmed that the candidate functional variants identified in IMF-specific *cis*-regulatory elements were indeed primarily associated with IMF-related meat quality traits (Fig. 5D).

In addition, given that genome sequence disparities have been implicated in the differences in backfat thickness and IMF content between MS and LW pigs [49], we further identified 218 and 307 candidate functional variants located at the top 10% of F_{ST} genomic regions between MS and LW pigs in specially active *cis*-regulatory elements of backfat and IMF, respectively (Fig. 5C). We next used pig ADSCs to validate the candidate functional variants of categories 1–2 SNPs [48] exist in two enhancers and one promoter that is uniquely activated in IMF. The dual-fluorescence reporter results indicated that categories 1–2 SNP mutations in enhancers of *HDAC4* and *PCK1* genes, as well as in promoter of *AGBL5* gene, tended to affect the transcriptional activity of these regulatory elements (Fig. 5E & S6A-6B). As these variants were linked to epigenetic regulation that varies between backfat and IMF, they could be used as resources for increasing pig IMF content and reducing backfat thickness in breeding programs.

Pig backfat thickness-associated genes could serve as candidate genes for human obesity related traits

We observed the human obesity-related genes *SETD2* and *HACE1*, both of which are located on distinct

chromosomes between humans and pigs, are regulated by functional-conserved promoters and enhancers (refer to Methods) in adipose tissues between humans and pigs (Fig. 5F). Moreover, the H3K27ac signals in functional-conserved promoters and enhancers of these two genes were also detected in four adipose depots in pigs. The anatomical distribution of adipose depots in different body parts is closely associated with obesity risk in humans [50]. Given the limited availability of epigenetic data on adipose depots from different human body parts, we next analyzed the expression and *cis*-regulatory elements conservation between the pig and human, as the similar biology function of adipose depots between the pig and human. The next expression analysis showed that 83.57% (290/347) of human obesity-associated genes in the HPO database (https://hpo.jax.org/) were expressed (CPM > 1) in at least one pig adipose depot (Fig. 5G). To further explore transcriptional similarities, we compared the expression profiles of human obesity-related genes and pig backfat thickness-associated candidate genes across four adipose depots. Using muscle tissue as a control, we classified human obesity-associated genes and pig backfat thickness-associated candidate genes into five groups: specific high expression in subcutaneous fat (includes backfat and belly fat), specific high expression in groin fat, specific high expression in IMF, low expression in all adipose depots (muscle specific), and high expression in all adipose depots. Our results suggested each group contained 4.69–28.57% of the highly expressed pig backfat thickness-associated candidate genes and 71.43–95.31% of highly expressed human obesity-associated genes, respectively (Fig. 5H).

In addition, we found that 19.03% of enhancers and 53.15% of promoters of human obesity-associated genes were functional conserved between the pig adipose depots and human adipose tissue (Fig. 5I). Moreover, 5.88% of enhancers and 48.39% of promoters of pig backfat thickness-associated candidate genes were functional conserved between pig adipose depots and human adipose tissue (Fig. S6C). Further analysis revealed the expression levels of human obesity-related genes in human adipose tissue were positively correlated with their expression in the four adipose depots of pigs (Fig. 5J). Concordantly, similar H3K27ac modification patterns around these genes were observed in adipose tissues between humans and pigs (Fig. 5K). Dual-fluorescence reporter assays of three randomly selected pig promoters conserved between pigs and humans demonstrated robust activation in both pig primary ADSCs and human ADSCs line (Fig. 5L & M). Consistently, additional reporter assays in pig PK-15 and human HEK-293 T cells also demonstrated their conserved regulatory potential across pigs and humans (Fig. S6D & E).

Overall, these results emphasized that the conserved transcriptional and epigenetic landscapes of human obesity-related genes between human adipose tissue and all adipose depots of pigs, indicating pig adipose depots may serve as valuable models for understanding human obesity related traits. Moreover, the functional conservation of *cis*-regulatory elements associated with backfat thickness loci in pigs highlights their potential as candidate genes for elucidating the genetic basis of human obesity.

Discussion

In this study, we conducted a comprehensive analysis of *cis*-regulatory elements across four adipose depots (backfat, belly fat, groin fat, and IMF) obtained from adult MS pigs. We generated H3K27ac ChIP-seq and ATAC-seq epigenomic datasets for these adipose depots, along with RNA-seq data, and additionally produced Hi-C genomic conformation datasets specifically for backfat and groin fat. In each depot, we identified over 20,000 enhancers and promoters, and more than 100,000 open chromatin regions. Overall, compared with previous studies [11, 16], 31.26% (enhancers), 10.90% (promoters), and 42.23% (open chromatin regions) of *cis*-regulatory elements were newly identified, respectively. This significantly enhances our understanding of the epigenomic landscape of adipose tissue and its regulatory control of gene expression in pigs.

Identifying variable *cis*-regulatory elements is crucial for understanding the specificity of regulation across different adipose depots. Here, H3K27ac profiling revealed minimal differences between belly fat and backfat, reflecting a high degree of epigenomic similarity between these subcutaneous depots. By contrast, substantial divergence in H3K27ac enrichment was observed between belly fat and groin fat, as well as between belly fat and IMF. Specifically, the comparison between belly fat and groin fat identified a group of well-established lipid synthesis-promoting genes, including *CD36* [29], *CEBPA* [51], *FABP4* [27], *PPARG* [26] and *SCD* [25], which were highly expressed in both backfat and belly fat. These results support the enhanced lipogenic potential of subcutaneous depots compared with groin fat, which shares similarities in transcriptomes with visceral fat [3].

In addition, SEs are known as major drivers of the transcriptional activation of cell identity genes [28], and our analysis underscored depot-specific SE-regulatory differences, with groin fat showing the highest number of switched SEs. Genes associated with these SEs had higher expressions in groin fat, including adipocyte differentiation promoting genes *LGMN* [33], *ID2* [32] and *KLF4* [31]. Together, these findings indicate that backfat and belly fat are more strongly associated with lipid synthesis and fat deposition, whereas groin fat is more closely linked to adipocyte differentiation.

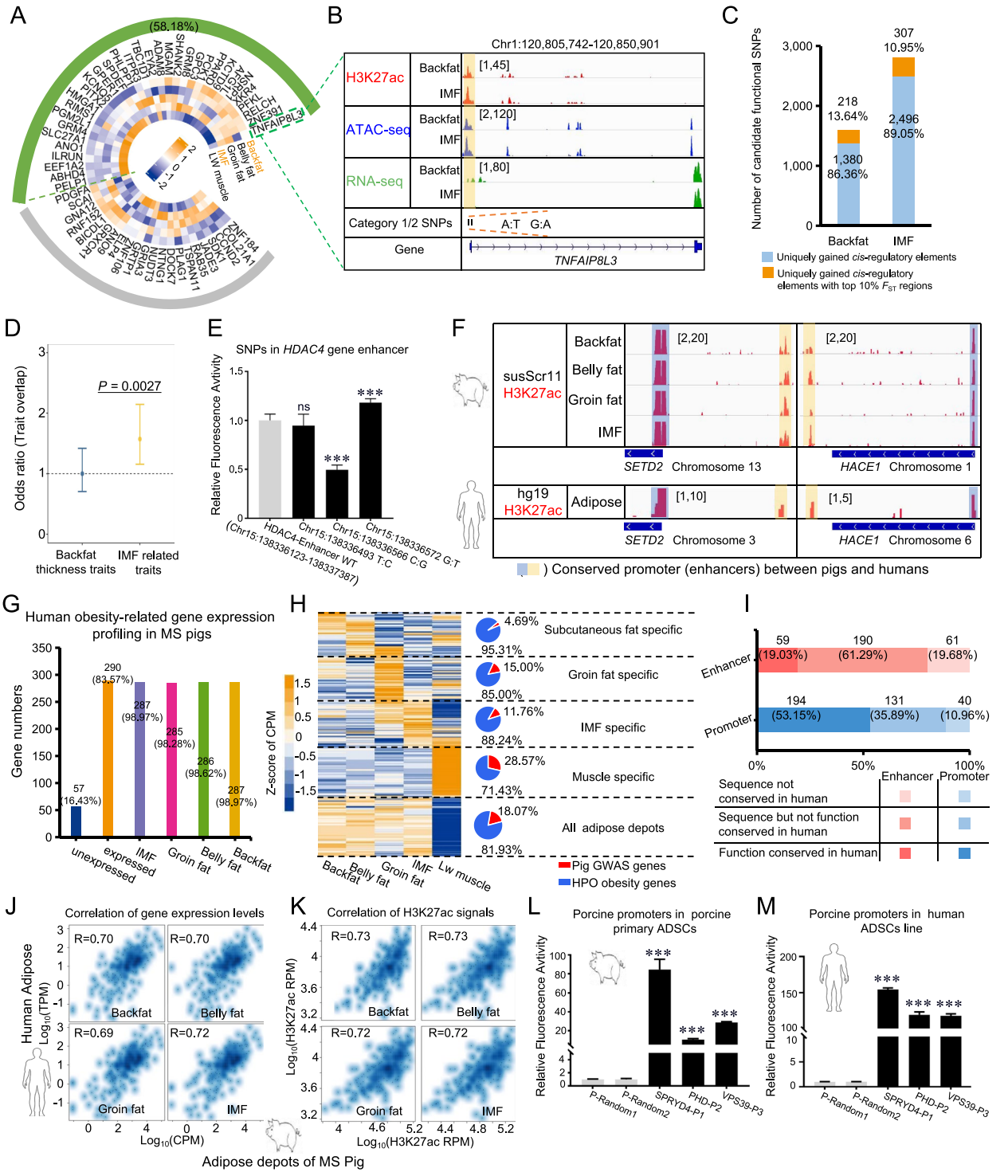

Fig. 5 (See legend on next page.)

Transcription factors regulate gene expression by binding to *cis*-regulatory elements. We identified 29 TFs that were consistently expressed across four adipose depots, participating in core regulatory programs essential for adipose biology. Notably, we also observed distinct TF binding patterns across four adipose depots. In belly fat, ESSRB, SOX6, PGR, and PPARA were selectively enriched in depot-specific activated *cis*-regulatory elements and were highly expressed, consistent with their known roles in promoting adipocyte hypertrophy and

(See figure on previous page.)

Fig. 5 Analysis of pig backfat thickness-associated gene and human obesity-associated genes and identification of candidate functional SNPs. **A** Expression heatmap of backfat thickness-associated candidate genes in four different adipose depots and LW muscle tissue (as a control). **B** H3K27ac ChIP-seq, ATAC-seq, and RNA-seq intensities and genomic variants (with high/moderate confidence of disrupting TF binding) around the *TNFAIP8L3* gene in backfat and IMF. **C** The number and percentage of pig candidate functional SNPs located within F_{ST} regions and *cis*-regulatory elements with gained H3K27ac modifications in backfat and IMF, respectively. **D** Odds ratio from Fisher's exact test was calculated for variants associated with H3K27ac peaks in four adipose depots and uniquely gained H3K27ac peaks in IMF across backfat thickness trait and IMF content trait. **E** Dual-luciferase reporter assay was used to validate the effects of categories 1–2 SNPs on the regulatory elements activity in pig primary adipose cells (ADSCs). **F** H3K27ac signals in the promoters and enhancers of the *SETD2* and *HACE1* genes in the four adipose depots from MS pigs and human adipose tissue. **G** Expression of human obesity-associated genes from the HPO database in pig adipose depots. **H** The expression of human obesity-associated genes and pig backfat thickness-associated candidate genes in the four adipose depots of MS pigs and LW muscle tissue (as a control). The pie chart shows the percentage of backfat thickness-associated candidate genes or human obesity-associated genes in each group. **I***Cis*-regulatory elements sequence and function conservation analysis between pigs and humans. The genes used for conservation analysis are pig adipose depots-expressed human obesity-associated genes in PHO database. **J** Correlation analysis of human obesity-associated genes expression between human adipose tissue and each pig adipose depot. The x-axis shows the gene expression level (CPM) in each adipose depot from MS pigs, and the y-axis shows the gene expression level (TPM) in adipose tissues from humans. PPC presents pearson correlation coefficient (PCC). **K** Correlation analysis of H3K27ac intensity around human obesity-associated genes between human adipose tissue and each adipose depot from MS pigs. The x-axis shows the H3K27ac intensity for each adipose depot from MS pigs, and the y-axis shows the H3K27ac intensity in human adipose tissues. **L**-**M** Verification of pig promoter activity in pig primary ADSCs and human ADSCs line using dual-fluorescence reporter system. *P*-random1 and 2 were negative controls. The *P*-value in figure **E** & **L**-**M** was calculated using Student's t-test, and the data are mean ± standard deviation (n = 4), with *** indicating $P < 0.001$, ns indicating no significant difference.

lipid accumulation [36, 52–54]. Notably, PGR has previously been reported to display lineage-specific expression patterns between the basal and luminal lineages in the mouse mammary gland, where it maintains chromatin interactions and sustain target gene expression [55]. Similarly, KLF4 and FOSL2 were uniquely enriched in groin fat. KLF4 is known to activate *C/EBPβ*, a master regulator of adipocyte differentiation [31], while FOSL2 regulates early differentiation markers such as *LEP* [56]. Intriguingly, HOXA10 and HOXA13, classically associated with muscle development [39, 57], were selectively enriched in IMF specific-activated *cis*-regulatory elements and displayed high expression levels, suggesting a potential crosstalk between IMF and adjacent muscle tissue. Collectively, the spatially specific expression and binding of adipocyte-specific transcription factors are likely to contribute to these depot-specific chromatin state disparities and functional specialization.

GWAS studies have shown that over 90% of trait-related SNPs reside in non-coding regions, emphasizing the role of regulatory element mutations in phenotypic variation [58]. Similarly, SNPs located near enhancers have been associated with the genetic control of complex traits in pigs [59]. Here, we identified a great number of SNPs with potential functional significance and are located on regulatory elements associated with traits like backfat thickness and IMF content. Trait enrichment analysis revealed a greater enrichment of SNPs related to meat quality traits in IMF compared to backfat. These results underscore the importance of integrating epigenomic and genomic data to identify variants relevant to economically important traits. Genomic selection (GS) is a widely used approach for improving traits in livestock breeding [60]. However, enhancing the accuracy of genomic estimated breeding values (GEBVs) has been a major challenge in GS. Recent evidence suggests that incorporating functional variants into GS models enhances the reliability of GEBVs compared to those based on randomly selected SNPs [48]. Thus, the *cis*-regulatory elements-associated variants identified here offer practical utility for breeding programs aimed at increasing IMF content and reducing backfat thickness, providing a molecular foundation for precision trait selection.

Evolutionary studies have uncovered the widespread conservation of *cis*-regulatory elements and transcription factors binding sites across human and other mammalian species [61]. Consistent with these findings, we identified functionally conserved enhancers and promoters associated with human obesity and pig backfat thickness genes in adipose tissues. In brief, H3K27ac modification landscapes at obesity-related loci were positively correlated between human and pig orthologues, which also exhibited comparable expression profiles. Moreover, regulatory elements associated with pig backfat thickness-associated candidate genes identified through GWAS showed similar activity across species. These results suggesting that porcine adipose tissues may serve as valuable models for human obesity research and candidate genes associated with pig backfat thickness may also represent conserved targets relevant to human obesity, offering promising avenues for future investigation into the molecular underpinnings of adipose biology and metabolic disease.

Materials and methods

Sample collection, library construction, and sequencing

Pig adipose tissue collection

Backfat, belly fat, groin fat, and IMF tissues were collected from two unrelated 6-month-old male MS pigs and stored at − 80 °C after snap-freezing in liquid nitrogen. Belly fat and IMF tissues from adult DLY (Duroc × Landrace × Yorkshire) three-way crossbred pigs were used for RT-qPCR validation. All experimental sample collection

processes were approved by the Ethics Committee of Huazhong Agricultural University (HZAUSW-2018-008).

RNA-seq library construction and sequencing

Total RNA was extracted from four adipose tissues, each sampled from two MS pigs, using TRIzol reagent (Thermo Scientific, 15596026). The RNA samples had high quality with RNA integrity values of 6.4–8.5 (Supplementary Table 1). The high-quality RNA samples were further purified using the rRNA-depletion method (Ribo-Zero-Seq) and used to construct strand-specific RNA-seq libraries in accordance with the Illumina guidelines (Illumina, San Diego, CA). The libraries were sequenced using the Illumina HiSeq X Ten (PE150) platform, and 30.8–45.9 M raw reads were acquired for each sample.

ChIP-seq library construction and sequencing

For immunoprecipitation of DNA for ChIP-seq library construction, the frozen adipose tissues were ground to a fine powder in liquid nitrogen, and about 400 mg adipose tissue, an amount sufficient for two ChIP-seq experiments, was transferred to a 15 ml centrifuge tube (Corning, 430052) and resuspended with 5 ml cold phosphate-buffered saline (PBS). The adipose tissue was fixed with 1% formaldehyde (Sigma-Aldrich, 252549) while rotating at room temperature for 20 min. To quench the fixation, glycine was added to a final concentration of 0.2 M, and the sample was rotated at room temperature for 10 min. The fixed adipose tissue was washed with cold PBS and divided into two 1.5 ml microtubes (Axygen, MCT-150-C), then quickly frozen in liquid nitrogen. Samples were stored at − 80 °C or used immediately for the next step. Nuclei were released with lysis buffer (1% SDS, 50 mM Tris-HCI [pH 8.0], 20 mM EDTA, 1 × protease inhibitors), and the nuclear lysates were fragmented using a Covaris S220 (Adaptive Focused Acoustics®); 0.5–1.0 μg DNA was acquired for immunoprecipitation. H3K27ac (Abcam Cat# ab4729, RRID: AB_2118291) antibodies (3 μg) were added to 11 μl M-280 sheep anti-rabbit IgG Dyna beads (ThermoFisher, 11203D), and then was rotated at 4 °C overnight. After that, incubating the mixture of chromatin and antibody-bound beads at 4 °C overnight. Then ChIP-DNA was purified and ChIP-seq libraries were constructed as described by the NEB Next® Ultra™ II DNA Library Prep Kit (NEB #E7645S/L), and then sequenced on an Illumina HiSeq X Ten PE150 platform.

ATAC-seq library construction and sequencing

About 50 mg of each adipose tissue was washed with 1 ml ice-cold PBS and then nuclei were released in 1 ml lysis buffer (50 mM HEPES [pH 7.5] [Life Technologies, 15630–080], 140 mM NaCl [Ambion, AM9760G], 1 mM EDTA [pH 8.0] [Ambion, AM9260G], 10% glycerol [Sigma-Aldrich, G7757], 0.5% NP-40 [Roche, 11754599001], and 0.25% Triton X-100 [Amresco, 0694]) by rotating at 4 °C for 10 min followed by washing with 1 ml cold PBS. Nuclei were filtered with a 40 μm cell strainer, and the number of nuclei were counted. The transposition reaction mixture (12.5 μl TD buffer, 10 μl ddH_2O, and 2.5 μl TDE [Illumina, FC-121-1030]) was added to 50,000 nuclei, and the reaction was incubated at 37 °C with shaking (650 rpm) for 1 h in a Thermo Mixer (Eppendorf). DNA purification was then performed with a DNA Clean&Concentrator-5 kit (ZYME, D4004). PCR amplification was carried out with an appropriate number of cycles, which was determined to nine according to our previous research. Size selection of the amplified PCR products (200–1000 bp fragments) was performed with KAPA pure beads (Roche, KS8002). Products from the size selection step were quantified and sequenced using an Illumina HiSeq X Ten PE150 platform.

Hi–C 3.0 library construction and sequencing

We constructed Hi-C 3.0 libraries for backfat and groin fat of MS pigs according to the standard protocol with several modifications [1]. In this study, adipose tissues were fixed with 1% FA (F8775, Sigma) and 2.5 mM EGS (21,565, Thermo Scientific), and restriction enzymes AluI (R0137, NEB) and HaeIII (R0108, NEB) were used to digest chromatin, and biotin-labled bridge linker were used for proximal ligation. To capture as many genomic chromatin interaction events as possible, we invested 600 ng of DNA derived from proximal ligation for subsequent library construction. For each library, approximately 200 G of raw sequencing data was obtained.

Sequencing data processing

RNA-seq

The reads obtained from RNA-seq were aligned to the susScr11 (*Sus scrofa* 11.1) reference genome assembly using STAR v2.7.5c. RSEM v1.3.3 was used to calculate gene expression levels with the GTF form Ensembl Release 101 used as input Genes that were not simultaneously detected in two replicates were removed, and the counts per million (CPM) profiles of genes were obtained using DESeq2 v1.36.0. DEGs between different adipose depots were also identified using DESeq2 with |log2FoldChange| (|log2FC|) > 1 and $P < 0.05$. Although IMF had only one replicate, DESeq2 allows such comparisons when other conditions include replicates, as was the case for backfat, belly fat, and groin fat. These depots had sufficient replicates to estimate dispersion, enabling valid differential expression analysis involving IMF. For gene expression filtering, we required CPM > 1 in at least two replicates for depots with replicates, while for IMF (with only one replicate), we applied the threshold of

CPM > 1 in that single sample. DEGs between groin fat and belly fat tissue, and those between IMF and belly fat tissue were subjected to gene ontology (GO) term analysis using DAVID Bioinformatics Resources 2021 (https://david.ncifcrf.gov/). The lipid synthesis-promoting genes derived from the DEGs in the GO terms.

ChIP-seq

ChIP-seq datasets were processed according to the ENCODE ChIPseq pipeline (https://github.com/kundajelab/chipseq_pipeline). In addition, the H3K27ac datasets of adipose tissues from adult LW pigs were downloaded from GEO under accession number GSE158418 (http://ncbi.nlm.nih.gov/geo).

The cross-correlation values, including NSCs and RSCs, were calculated for each sample via the ENCODE ChIP-seq pipeline. The FRiP scores were calculated based on read counts (FRiP = reads falling into peak regions/total mapped reads). All ChIP-seq samples with NSC > 1.05, RSC > 0.8, and FRiP > 1% were considered qualified [62]. Narrow peaks with $P > 10^{-5}$ and (IP_{RPM}-$INPUT_{RPM}$) < 1 were removed, the overlapping of enriched regions was merged, and then the 2 kb regions centered at the midpoint of merged regions were acquired to identify enhancers and promoters.

The promoters and enhancers of different adipose depots from MS pigs were identified using the trimethylation of histone H3 at lysine 4 (H3K4me3) and H3K27ac ChIP-seq data from a previous study [11], as well as H3K27ac ChIP-seq data from MS pigs generated here. The regions enriched with both H3K27ac signal located within the extended regions (2.5 kb upstream and 1 kb downstream) of a gene transcription start site (TSS) from our previous study [11] and H3K4me3 signals were designated as promoters, and other H3K27ac peaks were defined as potential enhancers.

Super-enhancers (SEs) in each fat tissue were identified in accordance with the default parameters of ROSE from the Young Lab [28]. Furthermore, to characterize the resemblance and discrepancy between the epigenomes of different fat depots of MS pigs, the overlap between H3K27ac peaks identified by ChIP-seq data from the four different fat tissues was investigated using Intervene v0.6.5. To calculate the H3K27ac signal matrix of enhancers and promoters in the four fat depots of MS, the enhancer and promoter regions identified by ChIP-seq data were separately merged using the merge command of BEDTools v2.26.0 with the parameter "–d 0". The multiBigwigSummary BED-file function of deepTools v2.5.2 was utilized to calculate the H3K27ac intensity of merged enhancers and promoters in different MS fat depots.

The normalize.quantiles function of the preprocessCore package v1.58.0 in R v4.2.1 was used to normalize the H3K27ac signals, which were used for generating heatmaps. The heatmaps of enhancers and promoters showing distinct patterns of H3K27ac intensity between different MS fat tissues were generated by clustering using the k-means function and plotting using the pheatmap package v1.0.12 in R v4.2.1. In the H3K27ac intensity heatmap of enhancers and promoters of backfat, belly fat, groin fat, and IMF, enhancers of clusters P19–P20 and promoters of clusters P19–P20 were defined as stable. Enhancers of cluster P20 and promoters of clusters P20 showed high H3K27ac intensities in all fat samples. Housekeeping genes regulated by enhancers or promoters of P20 were filtered out, and the filtered genes were subjected to GO term enrichment analysis using DAVID Bioinformatics Resources 2021 (https://david.ncifcrf.gov/), using a significance threshold of $P < 0.05$. The housekeeping genes were identified using transcriptomes of 12 tissue types from four pig breeds of 2-week-old pigs in previous research [11], and the housekeeping gene list is presented in Supplementary Table 11.

ATAC-seq

ATAC-seq datasets from this study and those of adipose tissue from adult LW pigs downloaded from GEO (accession number GSE158418; http://ncbi.nlm.nih.gov/geo) [16] were processed in accordance with our previous study [11]. The broad peaks of ATAC-seq signals of each fat tissue from MS pigs were called by the MACS2 v2.2.7.1 broad module, and a significant broad peak was defined as $P < 10^{-5}$. The footprints of each significant broad peak were analyzed using the wellington_footprints.py function of pyDNase v0.2.0 with the parameters "–A" and a significance threshold of $P < 10^{-15}$. The overlap between open chromatin regions identified by ATAC-seq data for the four different fat depots from MS pigs was determined using Intervene v0.6.5.

To characterize the differential open chromatin regions, the overlapping open chromatin regions between different adipose depots were identified using the intersect command of BEDTools v2.26.0 with the parameter "–d 0". The overlap between the merged open chromatin regions and H3K27ac peaks was determined using BEDTools v2.26.0. The multiBigwigSummary BED-file function of deepTools v2.5.2 was used to calculate the ATAC intensities of merged open chromatin regions in belly fat, groin fat, and IMF. The ATAC intensities were normalized using the normalize.quantiles function of the preprocessCore package v1.58.0 in R v4.2.1 (https://bioconductor.org/packages/preprocessCore) and used for gene rating heatmaps of merged open chromatin regions.

Comparative analysis of cis-regulatory elements

We merged the promoters, enhancers, H3K27ac peaks, and open chromatin regions from published data (from the adipose depots of 2-week-old pigs and adult LW

pigs) using BEDTools, respectively. The *cis*-regulatory elements (promoters, enhancers, and open chromatin regions) identified in the backfat, belly fat, groin fat, and IMF of MS pigs were also merged, respectively. The overlap between these merged *cis*-regulatory elements of MS pigs and those *cis*-regulatory elements of published data was determined using the intersect command of BEDTools. In addition, the overlap of H3K27ac peaks and open chromatin regions between each adipose depot from this study and those from published data was determined, respectively.

Hi–C

The TADs and Hi-C contact matrixes of two adipose tissues, ULB and GOM of Bama pig, were downloaded from GEO under accession number GSE183447 (http://ncbi.nlm.nih.gov/geo). The analysis of changes in TADs was mostly based on a previous study [23]. The TADs of the ULB that uniquely overlapped with those in the GOM were identified, and a TAD was defined as a stable TAD when the ratio of overlap was 0.5. TADs in the ULB that were split into two or more TADs in the GOM were defined as split TADs. The TADs that were present as two or more TADs in the ULB but present as a single TAD in the GOM were defined as merged TADs, and the remaining changes were classified as TAD rearrangements [23].

For the stable and changed TADs (i.e., those that differed between the ULB and GOM), the H3K27ac and ATAC-seq peak intensities of each MS fat depot were calculated. The multiBigwigSummary BED-file function of deepTools v2.5.2 was utilized to calculate the H3K27ac and ATAC-seq intensities of the backfat for stable and changed TADs. The H3K27ac and ATAC-seq intensities were normalized using the normalize.quantiles function of the preprocessCore package v1.58.0 in R. The normalized H3K27ac and ATAC intensities of TADs were used for generating boxplots. Moreover, the number of differential H3K27ac modification peaks between different fat depots that overlapped with the stable or changed TADs were counted.

The Hi-C 3.0 data of backfat and groin fat were processed using the HiC-Pro (version 2.11.1) pipeline to produce the ICE normalization contact matrices. The insulation score of the ICE matrix was calculated by using the following options: -is 480,000 -ids 320,000 -im iqrMean -ss 160,000. Furthermore, the insulation method was utilized to define the topologically associating domain (TAD) structure (insulation/boundaries). The methods for stable and changed TADs between backfat and groin fat were consistent with those used for ULB and GOM.

Analysis of differentially activated cis-regulatory elements

The enhancers and promoters between backfat and belly fat, backfat and groin fat, backfat and IMF, belly fat and groin fat, belly fat and IMF, and groin fat and IMF were merged by BEDTools v2.26.0 respectively. EdgeR v3.38.4 was used to identify the differentially activated promoters or enhancers with $|\log_2 FC| > 0.58$ and $P < 0.05$. The distance from each enhancer to the TSS of each gene was calculated in the range of ± 500 kb centered on the enhancer. The gene closest to an enhancer was considered to be potentially regulated by that enhancer, and the gene and its enhancer were located in the same TAD. Furthermore, if a promoter overlapped with the TSS region of a gene, that gene was considered to be regulated by that promoter.

The differentially activated open chromatin regions (between belly fat and groin fat and between belly fat and IMF) were similarly identified by edgeR with the criteria $|\log_2 FC| > 0.58$ and $P < 0.05$. The regulatory genes in open chromatin regions were identified using the same methods used to identify enhancers. Then the differentially activated enhancers, promoters, and open chromatin regions were separated into two groups according to the $\log_2 FC$ value, and the *cis*-regulatory elements without differential histone modification were selected as controls. The $\log_2 FC$ expression values of genes associated the *cis*-regulatory elements were compared using the wilcox.test function in R v4.2.1.

Moreover, the number of footprints in each ATAC-seq broad peak for different fat depots (belly fat and groin fat, belly fat and IMF) was counted, and the ATAC broad peaks in different fat depots (belly fat and groin fat, belly fat and IMF) were merged using BEDTools v2.26.0. The number of footprints represents the number of transcription factors (TFs). The TF number in the merged peaks between belly fat and groin fat or belly fat and IMF were compared, and peaks with the same number of TFs in the two depots were considered stable peaks. If the numbers of TFs were different between two adipose depots, the merged peaks were separated into two groups (increased or decreased number of TFs) based on the positive or negative values of subtraction result of the two numbers.

The *cis*-regulatory elements were classified by determining the overlap between each category ATAC broad peak and the log2FC of H3K27ac signal in the *cis*-regulatory elements, and the associated each category ATAC broad peak was compared by wilcox.test function in R v4.2.1. The overlap between the merged ATAC-seq peaks (belly fat and groin fat, or belly fat and IMF) and the merged H3K27ac peaks was determined. The "computeMatrix scale-regions" function of deepTools v2.5.2 was utilized to calculate the H3K27ac (or ATAC-seq) intensities of belly fat and groin fat (or belly fat and IMF) for overlapping peaks with the parameters "–binSize 100

–beforeRegionStartLength 5000–afterRegionStartLength 5000–regionBodyLength 100".

Analysis of super-enhancers in four different adipose depots

To validate the reliability of SEs, the SE score, calculated by ROSE, of these defined as SEs was compared with these of an equal number of random enhancers. Moreover, the SEs and TEs from four different adipose tissues and the expression profiles of genes associated with them were applied for statistical comparisons. The regulated genes associated with SEs were identified in accordance with enhancers. To annotate the GO biological process terms of genes associated with SEs in backfat, belly fat, groin fat, and IMF, GO analysis was conducted using DAVID Bioinformatics Resources 2021 (https://david.ncifcrf.gov/), using a significance threshold of $P < 0.05$.

ROSE was used to merge the enhancers of the four different adipose depots for identifying the SEs. We ranked the merged enhancers according to SE score in backfat, belly fat, groin fat, and IMF. The merged enhancers identified as SEs in all four adipose depots were defined as stable SEs; the merged enhancers identified as an SE in any three of the four adipose depots were defined as "stable at least in three adipose depots"; and the merged enhancers identified as SEs in no more than two of the four adipose depots were defined as "SEs switched at least in two adipose depots" or "swiched SEs".

Motif analysis of transcription factors

The TFs of footprints on merged open chromatin regions between belly fat and groin fat and between belly fat and IMF were identified using the findMotifs.pl function of HOMER v4.11.1 with $P < 0.01$. These TFs were first filtered by gene expression profile, and the differentially expressed TFs are highlighted in the figures. We determined the overlap between expressed TFs of footprints on open chromatin regions with up-regulated H3K27ac signals in belly fat (compared with groin fat or IMF) and those of footprints on open chromatin regions with down-regulated H3K27ac signals in belly fat (compared with groin fat or IMF). These overlapping TFs were defined as changed TFs of changed peaks between different adipose depots.

In the H3K27ac intensity heatmap of enhancers and promoters in backfat, belly fat, groin fat, and IMF, enhancers of clusters P19–P20 and promoters of clusters P19–P20 were defined as shared enhancers and promoters among the four adipose depots. The H3K27ac intensities of these shared enhancers and promoters were calculated using the "computeMatrix scale-regions" function of deepTools v2.5.2. After filtering out the differentially activated promoters/enhancers and these associated with housekeeping genes, the remaining promoters/enhancers were defined as stable promoters/enhancers. Then the overlap between the stable promoters or enhancers and the open chromatin regions were determined, and the overlapped open chromatin regions were defined as stable open chromatin regions. Motif analysis was conducted on footprints of stable open chromatin regions. The predicted TFs binding on stable open chromatin regions was defined as stable TFs on stable peaks; the housekeeping genes and changed TFs were removed, and those with CPM > 1 in at least one adipose depot were retained.

Conservation analysis of cis-regulatory elements across mammals

The backfat thickness-related genes were collected from Web of Science. The F_{ST} value between LW (n = 37) and MS (n = 16) was calculated by VCFtools v0.1.17 with parameters "–fst-window-size 150,000–fst-window-step 15,000" [63]. Furthermore, the number of Category 1 and Category 2 SNPs of pig in H3K27ac-activated peaks from four different fat depots were counted [48], these SNPs were also located in top 10% F_{ST} regions. QTLs of backfat thickness traits and IMF traits for pig were downloaded from PigQTLdb database (https://www.animalgenome.org/cgi-bin/QTLdb/SS/index/). The number of functional variants associated with QTLs for backfat thickness traits and IMF related traits (unpublished data) in our H3K27ac-activated peaks from four different fat depots was counted. We identified the obesity-related genes with the term HP: 0001513 from the Human Phenotype Ontology (HPO, https://hpo.jax.org/app/). The names of HPO genes were converted to the names of the homologous genes in pigs. In addition, these genes were filtered by the gene expression profile in MS fat tissues. Heatmaps of the expression levels of backfat thickness-related genes and both obesity- and backfat thickness-related genes were generated using the pheatmap package v1.0.12.

Human ChIP-seq data for H3K27ac were downloaded from the Roadmap Epigenomics project (Roadmap Epigenomics [wustl.edu]). The 1 kb regions centered on each predicted promoter and enhancer from obesity-related genes were converted from pig genomic locations (susScr11) to human genomic locations (hg19) using the LiftOver tool from the UCSC genome browser with the parameter "minMatch = 0.5". The pig enhancers and promoters that could be converted to human genomic locations were considered as sequence-conserved enhancers and promoters. Furthermore, the enhancers and promoters of pigs were considered function conserved if the corresponding human homologous sequence was covered by human enhancers and promoters, respectively. The covered reads in the range of ± 500 kb centered on the TSS regions of obesity-related genes were calculated using the multiBamSummary BED-file function of deepTools2.5.2.

Cell experiments

Isolation of pig adipose-derived stem cells (ADSCs)

The dissociation protocol was adapted from prior research with minor adjustments [64]. ADSCs from porcine backfat of 2-day-old piglets were collected and minced with scissors. Then digested in a solution containing collagenase A (ROCHE, 10103586001), dispase II (ROCHE, 4942078001), and 2% AA (Gibco, 15140122) prepared in DMEM (Gibco, C11995500BT). Digestion was performed in water bath shaker at 37 °C for 1 h. Digestion was terminated by the addition of an equal volume of DMEM containing 2% AA, and the cells were resuspended in DMEM containing 20% FBS and 2% AA. The suspension was filtered through a 100 μm cell strainer. The collected ADSCs were cultured in growth medium as outlined below.

Cell cultures

For PK-15 and HEK-293 T cell culture, cells were cultured in basic culture medium DMEM (Gibco, C11995500BT) supplemented with 10% FBS (Gibco, 10270–106) at 37 °C in 5% CO_2. For primary pig ADSCs and human ADSCs line (IM-H289, IMMOCELL), cells were cultured in growth medium (Gibco, C11875500BT) supplemented with 20% FBS, 1% GlutaMax (Gibco, 35050061), 1% NEAA (Gibco, 11140050), 5 ng/ml bFGF (Gibco, 13256029), 1% AA (Gibco, 15140122) at 37 °C in 5% CO_2. For adipogenic differentiation of ADSCs, medium was formulated as previously described, with minor modifications made. When cells reached 80% confluence, they were treated with adipogenic induction medium (MAD I: 0.5 mM IBMX, 125 nM indomethacin, 1 μM dexamethasone, 20 nM insulin, 1 nM T3, and 0.5 μM rosiglitazone added to complete DMEM medium with 10% FBS) for 2 days. Then, the medium was switched to maintenance differentiation medium (MAD II: 20 nM insulin added to complete DMEM medium with 10% FBS) and cells were cultured for another 5 days before being harvested. Medium was changed every day.

Oil red O staining

To confirm the success of adipogenic induction, cells were fixed in 4% paraformaldehyde for 20 min at room temperature, then washed twice with PBS. Next, they were dehydrated in 60% isopropanol for 5 min and washed with PBS. After that, cells were incubated with Oil Red O (dissolved in 60% isopropanol) for 30 min, rinsed with 60% isopropanol for 5 s, and finally washed three times with PBS. Then observe the cells under a microscope and take photos.

Luciferase activity assay

The dual-luciferase reporter system was used to verify the *cis* regulatory elements activity and the effects of categories 1–2 SNPs on the regulatory elements activity. The promoters and the corresponding random regions (serving as negative controls) from the pig genome were cloned into PGL3-Basic vector plasmid (E1751, Promega), respectively. The enhancers and the corresponding random regions (serving as negative controls) from the pig genome were cloned into PGL3-Promoter vector plasmid (E1761, Promega), respectively. The genomic barren regions that were non-coding areas and showed no enrichment of H3K27ac or ATAC-seq signal in our datasets were used as negative controls. The cell transfection kit jetPrime (Polyplus, 101000046), fluorescence detection kit (11402ES60, Yeasen), as well as the multifunctional microplate reader (BioTek Synergy H1, Agilent) were used according to manufacturer's instructions. The genomic loci for the cloned sequences, along with the primer sequence information used in this study, are detailed in Supplementary Table 8, and the detailed insert sequences information are in Supplementary Table 12.

RT-qPCR assay

Total RNA was extracted using Trizol reagent (15596018CN, Invitrogen) and RNA extraction kit (ER501, Trans) from ADSCs isolated from the backfat tissue of two-day-old Large White pigs, as well as from adipocytes after their induction of adipogenic differentiation. The extracted mRNA was reverse-transcribed to generate cDNA (RR047A, TAKARA). The SYBR® Green Realtime PCR Master Mix (QPK-201, Toyobo) was used to detect mRNA levels by quantitative real-time PCR assayed on the real-time PCR detection system (Bio-Rad). The relative levels of RNA expression were normalized to GAPDH expression levels using the $2^{-\Delta\Delta Ct}$ method. Each sample was detected in quadruplicate. The genomic loci and primer sequences for RT-qPCR are shown in Supplementary Table 9.

SiRNA transfection experiment

To knockdown *PPARA* and *SOX6* genes, siRNAs targeting these two genes were purchased from Anhui Generalbiol. SiRNA or negative control were transfected into ADSCs using jetPrime (Polyplus, 101,000,046) according to the manufacturer's instructions. After 5 h, cells were washed once with PBS and cultured in adipogenic induction medium (MAD I). Cells were then cultured as described above for 72 h before being harvested. The siRNA sequences for *PPARA* and *SOX6* genes are shown in Supplementary Table 10.

Supplementary Information

The online version contains supplementary material available at https://doi.org/10.1186/s13578-025-01513-8.

Supplementary Material 1: Figure S1 Identification of cis-regulatory elements in four adipose depots. (A-C) Multidimensional scaling (MDS) analysis of various datasets. MDS analysis of H3K27ac ChIP-seq, RNA-seq, and ATAC-seq data for backfat, belly fat, groin fat, and IMF, respectively. (D-E) Statistical analysis of newly identified cis-regulatory elements for adipose tissues in this study. The published backfat data (blue) of four pig breeds (MS, ES, LW, and Duroc) at two weeks of age and adult LW pigs from FAANG project were used for comparing. (F-G) Verification of promoter and enhancer activities using dual-fluorescence reporter system in PK-15 cell lines. P/E-random were negative controls. The P-value was calculated using Student's t-test, and the data are mean ± standard deviation (n=4), with *** indicating P<0.001. (H) Venn diagram showing the overlap of open chromatin regions across four adipose depots. (I) Percentages of open chromatin regions identified in each adipose depot that are common to all, any three, any two, or only one depot, respectively. Figure S2 Distinct patterns of promoters for different adipose depots. (A) Heatmap of H3K27ac intensities in promoters for four adipose depots. (B) Venn diagram showing the overlap between genes associated with promoters in the P20 cluster and housekeeping genes. (C) Bar plot of enriched GO terms for P20-related genes excluding non-housekeeping genes. (D-E) Examples of genome browser screenshots showing the regions around the ID4 and MMP27 genes. Figure S3 Differential analysis in histone modification density and accessibility of cis-regulatory elements between belly fat and IMF. Venn diagram showing the overlap of TADs between the backfat and groin fat from MS pigs (A), as well as between ULB and the GOM from Bama pigs (B). Percentages of variable H3K27ac peaks located in stable or changed (other) TADs of MS pigs (C) and Bama pigs (D). (E) Distribution of variable H3K27ac signal peaks in stable and changed TADs of Bama pigs. Enrichment of ATAC signal intensity for each adipose depots at the boundaries of stable and changed TADs of MS pigs (F) and Bama pigs (H). (G) Enrichment of the H3K27ac modification intensity for each adipose depots at boundaries of stable and changed TADs of Bama pigs. (I) Volcano plot showing genes differentially expressed between belly fat and IMF. (J-L) Boxplot of the fold change (FC) in gene expression following differential histone modification of enhancers or promoters between adipose depots inside stable TADs of Bama pigs. Gain, stable and loss indicate changes of H3K27ac signal. (M). Boxplots indicating the fold change (FC) in H3K27ac signal densities of cis-regulatory elements following changes of footprint number between the belly fat and IMF inside stable TADs of Bama pigs. (N) Boxplot showing ATAC-seq intensity levels in enhancers of lipid synthesis-promoting genes differentially expressed across the four adipose depots inside stable TADs of Bama pigs. The P-values in (E-H), and (J-N) were calculated using a single-sided unpaired Wilcoxon test. * indicates P < 0.05, *** indicates P < 0.001. Figure S4 Bar plot of enriched GO terms for genes regulated by switched SEs. Figure S5 Enrichment of Transcription factors binding in belly fat and IMF. (A) Venn diagram showing the overlap of motifs enriched in footprints of cis-regulatory elements of belly fat gain and belly fat loss, respectively. Motifs of belly fat gain or loss represented that, compared with groin fat, motifs enriched in the cis-regulatory elements with H3K27ac and ATAC-seq signals simultaneously up-regulated or down-regulated in the belly fat, respectively. (B) Heatmap of H3K27ac and ATAC-seq intensities in cis-regulatory elements of belly fat and IMF. "Loss, stable and gain" represent differential H3K27ac or ATAC signals in cis-regulatory elements between the two adipose depots. (C) Venn diagram showing the overlap of motifs enriched in footprints of cis-regulatory elements in belly fat gain and belly fat loss, respectively. Motifs of belly fat gain or loss represent that, compared with IMF, motifs enriched in the cis-regulatory elements with H3K27ac and ATAC-seq signals simultaneously up-regulated or down-regulated in the belly fat, respectively. (D) Scatter plot of differentially expressed TFs that uniquely enriched in cis-regulatory elements of belly fat gain. (E) Logo plots and P values of motifs from TFs differentially expressed between belly fat and IMF. (F) Scatter plot of differentially expressed TFs that uniquely enriched in cis-regulatory elements of belly fat loss. (G) Logo plots and P values of motifs from TFs differentially expressed between belly fat and IMF. (H) Venn diagram illustrating the overlap of TFs with footprints in common cis-regulatory elements and those TFs with footprints in differential cis-regulatory elements between belly fat and groin fat, as well as between belly fat and IMF. (I-J) RT-qPCR validation of groin fat and IMF high expression genes in different depots, respectively. RT-qPCR validation of belly fat high expression genes (K) and IMF high expression genes (L) in the commercial three-way crossbred pigs (DLY). The data presented in I-L are mean ± standard deviation (n=3). The ns indicates not significant, * P<0.05, ** P<0.01, *** P<0.001. Figure S6 Conservation analysis and validation of cis-regulatory elements between pigs and humans. (A-B) Dual-luciferase reporter assay was used to validate the effects of categories 1-2 SNPs on the regulatory elements activity in pig primary adipose cells (ADSCs). The P-value in figures was calculated using Student's t-test, and the data are mean ± standard deviation (n=4), The ns indicates not significant, * P<0.05, ** P<0.01, *** P<0.001. (C) Sequence and function conservation analysis of promoters and enhancers for pig backfat thickness-associated candidate genes in adipose tissues between pigs and humans. (D-E) Verification of pig promoter activity in pig PK-15 and 293T cell lines using dual-fluorescence reporter system. P-random1 and 2 were negative controls. The P-value in figure A-B & D-E was calculated using Student's t-test, and the data are mean ± standard deviation (n=4), with *** indicating P<0.001, ** indicating P<0.01, * indicating P<0.05.

Supplementary Material 2.

Supplementary Material 3.

Supplementary Material 4.

Author contributions

M. Zhu, Y. Liao, and Y. Zhao conceived this study. D. Wang, X. Qi, H. Zhou, M. Hu, Y. Guo, and R. Ma collected the pig adipose tissues. D. Wang, Y. Shen, Z. Xu, and Y. Zhang conducted the library preparation for ChIP-seq, ATAC-seq, RNA-seq, and Hi-C. R. Kuang, M. H, J. Sun, Z. Han, and H. Peng were responsible for the data analysis. D. Wang and R. Kuang drafted the manuscript, while Y. Zhao and M. Zhu edited it. Y. Zhao, M. Zhu, Y. Liao, and Y. Zhao provided supervision for the study.

Funding

This research was supported by the National Key Research and Development Program of China (2021YFD1301201), the National Natural Science Foundation of China (32341051), the Natural Science Foundation of China (31961143020), the Hubei Provincial Foundation (HBZY2023B006-02), and the National Natural Science Foundation of China (3250200859).

Data availability

The raw sequence datasets generated in this study of ChIP-seq, ATAC-seq and RNA-seq data for each sample (with BioSample ID ranging from SAMN41637529 to SAMN41637536) have been deposited in the NCBI Sequence Read Archive (SRA) under the Bioproject accession number PRJNA597497. The ATAC-seq and H3K27ac ChIP-seq datasets of adipose tissues from adult LW pigs were downloaded from GEO under accession number GSE158418 (http://ncbi.nlm.nih.gov/geo). The H3K27ac ChIP-seq datasets of backfat from MS 2W pigs were downloaded from NCBI Sequence Read Archive (SRA) under the Bioproject accession number PRJNA597497. The TADs and Hi-C contact matrices of two adipose tissues, ULB and GOM of Bama pig, were downloaded from GEO under accession number GSE183447 (http://ncbi.nlm.nih.gov/geo). Human ChIP-seq data for H3K27ac were downloaded from the Roadmap Epigenomics project (Roadmap Epigenomics (wustl.edu)).

Declarations

Competing interests

The authors declare no competing interests.

Received: 19 May 2025 / Accepted: 16 November 2025
Published online: 26 November 2025

References

1. Lafontaine DL, Yang L, Dekker J, Gibcus JH. Hi-C 3.0: improved protocol for genome-wide chromosome conformation capture. Curr Protoc. 2021;1(7):e198.
2. Zwick RK, Guerrero-Juarez CF, Horsley V, Plikus MV. Anatomical, physiological, and functional diversity of adipose tissue. Cell Metab. 2018;27(1):68–83.
3. Sakers A, De Siqueira MK, Seale P, Villanueva CJ. Adipose-tissue plasticity in health and disease. Cell. 2022;185(3):419–46.
4. Petersen MCSG. Mechanisms of insulin action and insulin resistance. Physiol Rev. 2018;10:2133–223.
5. Guo Y, Hu M, Peng H, Zhang Y, Kuang R, Han Z, et al. Epigenomic features associated with body temperature stabilize tissues during cold exposure in cold-resistant pigs. J Genet Genomics. 2024;51(11):1252–64.
6. Wood JD, Enser M, Fisher AV, Nute GR, Sheard PR, Richardson RI, et al. Fat deposition, fatty acid composition and meat quality: a review. Meat Sci. 2008;78(4):343–58.
7. Ciobanu DC, Lonergan SM, Huff-Lonergan EJ: Genetics of meat quality and carcass traits: The genetics of the pig; 2011.
8. Zheng X, Zhao P, Yang K, Ning C, Wang H, Zhou L, et al. CNV analysis of Meishan pig by next-generation sequencing and effects of AHR gene CNV on pig reproductive traits. J Anim Sci Biotechnol. 2020;11(1):42.
9. Lunney JK, Van Goor A, Walker KE, Hailstock T, Franklin J, Dai C. Importance of the pig as a human biomedical model. Sci Transl Med. 2021;13(621):eabd5758.
10. Jin L, Tang Q, Hu S, Chen Z, Zhou X, Zeng B, et al. A pig BodyMap transcriptome reveals diverse tissue physiologies and evolutionary dynamics of transcription. Nat Commun. 2021;12(1):3715.
11. Zhao Y, Hou Y, Xu Y, Luan Y, Zhou H, Qi X, et al. A compendium and comparative epigenomics analysis of cis-regulatory elements in the pig genome. Nat Commun. 2021;12(1):2217.
12. Jin L, Wang D, Zhang J, Liu P, Wang Y, Lin Y, et al. Dynamic chromatin architecture of the porcine adipose tissues with weight gain and loss. Nat Commun. 2023;14(1):3457.
13. Clowney EJ, LeGros MA, Mosley CP, Clowney FG, Markenskoff-Papadimitriou EC, Myllys M, et al. Nuclear aggregation of olfactory receptor genes governs their monogenic expression. Cell. 2012;151(4):724–37.
14. Oudelaar AM, Higgs DR. The relationship between genome structure and function (vol 22, pg 154, 2021). Nat Rev Genet. 2021;12:22.
15. Tang ZH, Luo OJ, Li XW, Zheng MZ, Zhu JJ, Szalaj P, et al. CTCF-mediated human 3D genome architecture reveals chromatin topology for transcription. Cell. 2015;163(7):1611–27.
16. Kern C, Wang Y, Xu X, Pan Z, Halstead M, Chanthavixay G, et al. Functional annotations of three domestic animal genomes provide vital resources for comparative and agricultural research. Nat Commun. 2021;12(1):1821.
17. Wang Z, Zuo Z, Li L, Ren S, Gao T, Fu J, et al. Nrf2 in adipocytes. Arch Pharm Res. 2020;43(3):350–60.
18. Murad JM, Place CS, Ran C, Hekmatyar SK, Watson NP, Kauppinen RA, et al. Inhibitor of DNA binding 4 (ID4) regulation of adipocyte differentiation and adipose tissue formation in mice. J Biol Chem. 2010;285(31):24164–73.
19. Prasad V, Chirra S, Kohli R, Shull GE. NHE1 deficiency in liver: implications for non-alcoholic fatty liver disease. Biochem Biophys Res Commun. 2014;450(2):1027–31.
20. Zhu Z, Ali A, Wang J, Qi S, Hua Z, Ren H, et al. Myostatin increases the expression of matrix metalloproteinase genes to promote preadipocytes differentiation in pigs. Adipocyte. 2022;11(1):266–75.
21. Yue F, Cheng Y, Breschi A, Vierstra J, Wu W, Ryba T, et al. A comparative encyclopedia of DNA elements in the mouse genome. Nature. 2014;515(7527):355–64.
22. Nora EP, Goloborodko A, Valton AL, Gibcus JH, Uebersohn A, Abdennur N, et al. Targeted degradation of CTCF decouples local insulation of chromosome domains from genomic compartmentalization. Cell. 2017;169(5):930-944.e922.
23. Zhang J, Liu P, He M, Wang Y, Kui H, Jin L, et al. Reorganization of 3D genome architecture across wild boar and Bama pig adipose tissues. J Anim Sci Biotechnol. 2022;13(1):32.
24. Dragovich MA, Mor A. The SLAM family receptors: potential therapeutic targets for inflammatory and autoimmune diseases. Autoimmun Rev. 2018;17(7):674–82.
25. Tibori K, Zámbó V, Orosz G, Szelényi P, Sarnyai F, Tamási V, et al. Allele-specific effect of various dietary fatty acids and ETS1 transcription factor on SCD1 expression. Sci Rep. 2024;14(1):177.
26. Zhang Y, Li H. Three important transcription factors related to lipogenesis and adipogenesis in mammal. J Northeast Agric Univ. 2010;17:62–75.
27. Wang XW, Sun YJ, Chen X, Zhang WZ. Interleukin-4-induced FABP4 promotes lipogenesis in human skeletal muscle cells by activating the PPAR γ signaling pathway. Cell Biochem Biophys. 2022;80(2):355–66.
28. Whyte WA, Orlando DA, Hnisz D, Abraham BJ, Lin CY, Kagey MH, et al. Master transcription factors and mediator establish super-enhancers at key cell identity genes. Cell. 2013;153(2):307–19.
29. Smith J, Su X, El-Maghrabi R, Stahl PD, Abumrad NA. Opposite regulation of CD36 ubiquitination by fatty acids and insulin: effects on fatty acid uptake. J Biol Chem. 2008;283(20):13578–85.
30. Furuhashi M, Hotamisligil GS. Fatty acid-binding proteins: role in metabolic diseases and potential as drug targets. Nat Rev Drug Discov. 2008;7(6):489–503.
31. Birsoy K, Chen Z, Friedman J. Transcriptional regulation of adipogenesis by KLF4. Cell Metab. 2008;7(4):339–47.
32. Park KW, Waki H, Villanueva CJ, Monticelli LA, Hong C, Kang S, et al. Inhibitor of DNA binding 2 is a small molecule-inducible modulator of peroxisome proliferator-activated receptor-gamma expression and adipocyte differentiation. Mol Endocrinol. 2008;22(9):2038–48.
33. Jafari A, Qanie D, Andersen TL, Zhang Y, Chen L, Postert B, et al. Legumain regulates differentiation fate of human bone marrow stromal cells and is altered in postmenopausal osteoporosis. Stem Cell Rep. 2017;8(2):373–86.
34. Yu S, Wong YC, Wang XH, Ling MT, Ng CF, Chen S, et al. Orphan nuclear receptor estrogen-related receptor-beta suppresses in vitro and in vivo growth of prostate cancer cells via p21(WAF1/CIP1) induction and as a potential therapeutic target in prostate cancer. Oncogene. 2008;27(23):3313–28.
35. Du SY, Hu L, Zhou BH, Zhang Z, Li MC, Chang D, et al. Sox6 impairs the adipogenic commitment of mesenchymal stem cells by targeting lysyl oxidase and preadipocyte factor 1. Biochem Biophys Res Commun. 2023;681:225–31.
36. Leow SC, Poschmann J, Too PG, Yin J, Joseph R, McFarlane C, et al. The transcription factor SOX6 contributes to the developmental origins of obesity by promoting adipogenesis. Development. 2016;143(6):950–61.
37. Clavreul L, Bernard L, Cotte AK, Hennuyer N, Bourouh C, Devos C, et al. The ubiquitin-like modifier FAT10 is induced in MASLD and impairs the lipid-regulatory activity of PPARα. Metabolism. 2024;151:155720.
38. Bulut GB, Alencar GF, Owsiany KM, Nguyen AT, Karnewar S, Haskins RM, et al. KLF4 (Kruppel-like factor 4)-dependent perivascular plasticity contributes to adipose tissue inflammation. Arterioscler Thromb Vasc Biol. 2021;41(1):284–301.
39. Lin X, Yan M, Yu W, Ma Y, Zhang L, Wei W, et al. Hoxa11 and Hoxa13 facilitate slow-twitch muscle formation in C2C12 cells and indirectly affect the lipid deposition of 3T3-L1 cells. Anim Sci J. 2021;92(1):e13544.
40. Ullah K, Ai L, Humayun Z, Wu R. Targeting endothelial HIF2α/ARNT expression for ischemic heart disease therapy. Biology. 2023. https://doi.org/10.3390/biology12070995.
41. Pan X, Mota S, Zhang B. Circadian clock regulation on lipid metabolism and metabolic diseases. Adv Exp Med Biol. 2020;1276:53–66.
42. Wei J, Gao C, Lu C, Wang L, Dong D, Sun M. The E2F family: a ray of dawn in cardiomyopathy. Mol Cell Biochem. 2024. https://doi.org/10.1007/s11010-024-05063-4.
43. Cook ME, Jarjour NN, Lin CC, Edelson BT. Transcription factor Bhlhe40 in immunity and autoimmunity. Trends Immunol. 2020;41(11):1023–36.
44. Pinto K, Chetty R. Gene of the month: TFE 3. J Clin Pathol. 2020;73(11):691–4.
45. Chen H, Yu Z, Niu Y, Wang L, Xu K, Liu J. Research progress of PBX1 in developmental and regenerative medicine. Int J Med Sci. 2023;20(2):225–31.
46. Cui J, Hao C, Zhang W, Shao J, Zhang N, Zhang G, et al. Identical expression profiling of human and murine TIPE3 protein reveals links to its functions. J Histochem Cytochem. 2015;63(3):206–16.
47. Jiang Y, Tang S, Wang C, Wang Y, Qin Y, Wang Y, et al. A genome-wide association study of growth and fatness traits in two pig populations with different genetic backgrounds. J Anim Sci. 2018;96(3):806–16.
48. Ma R, Kuang R, Zhang J, Sun J, Xu Y, Zhou X, et al. Annotation and assessment of functional variants in livestock through epigenomic data. J Genet Genom. 2025. https://doi.org/10.1016/j.jgg.2025.03.013.
49. Nakajima I, Oe M, Ojima K, Muroya S, Shibata M, Chikuni K. Cellularity of developing subcutaneous adipose tissue in Landrace and Meishan pigs: adipocyte size differences between two breeds. Anim Sci J. 2011;82(1):144–9.
50. AlZaim I, de Rooij LPMH, Sheikh BN, Börgeson E, Kalucka J. The evolving functions of the vasculature in regulating adipose tissue biology in health and obesity. Nat Rev Endocrinol. 2023;19(12):691–707.

51. Tang QQ, Lane MD. Adipogenesis: from stem cell to adipocyte. Annu Rev Biochem. 2012;81(1):715–36.
52. Ijichi N, Ikeda K, Horie-Inoue K, Yagi K, Okazaki Y, Inoue S. Estrogen-related receptor alpha modulates the expression of adipogenesis-related genes during adipocyte differentiation. Biochem Biophys Res Commun. 2007;358(3):813–8.
53. Song T, Yang Y, Jiang S, Peng J. Novel insights into adipogenesis from the perspective of transcriptional and RNA N6-methyladenosine-mediated post-transcriptional regulation. Adv Sci. 2020;7(21):2001563.
54. Montagner A, Polizzi A, Fouché E, Ducheix S, Lippi Y, Lasserre F, et al. Liver PPARα is crucial for whole-body fatty acid homeostasis and is protective against NAFLD. Gut. 2016;65(7):1202–14.
55. Milevskiy MJG, Coughlan HD, Kane SR, Johanson TM, Kordafshari S, Chan WF, et al. Three-dimensional genome architecture coordinates key regulators of lineage specification in mammary epithelial cells. Cell Genom. 2023;3(11):100424.
56. Wrann CD, Eguchi J, Bozec A, Xu Z, Mikkelsen T, Gimble J, et al. FOSL2 promotes leptin gene expression in human and mouse adipocytes. J Clin Invest. 2012;122(3):1010–21.
57. Yoshioka K, Nagahisa H, Miura F, Araki H, Kamei Y, Kitajima Y, et al. Hoxa10 mediates positional memory to govern stem cell function in adult skeletal muscle. Sci Adv. 2021. https://doi.org/10.1126/sciadv.abd7924.
58. Khurana E, Fu Y, Chakravarty D, Demichelis F, Rubin MA, Gerstein M. Role of non-coding sequence variants in cancer. Nat Rev Genet. 2016;17(2):93–108.
59. Keel BN, Nonneman DJ, Lindholm-Perry AK, Oliver WT, Rohrer GA. Porcine single nucleotide polymorphisms and their functional effect: an update. BMC Res Notes. 2018;11(1):860.
60. Meuwissen TH, Hayes BJ, Goddard ME. Prediction of total genetic value using genome-wide dense marker maps. Genetics. 2001;157(4):1819–29.
61. Kuderna LFK, Ulirsch JC, Rashid S, Ameen M, Sundaram L, Hickey G, et al. Identification of constrained sequence elements across 239 primate genomes. Nature. 2024;625(7996):735–42.
62. Landt SG, Marinov GK, Kundaje A, Kheradpour P, Pauli F, Batzoglou S, et al. ChIP-seq guidelines and practices of the ENCODE and modENCODE consortia. Genome Res. 2012;22(9):1813–31.
63. Danecek P, Auton A, Abecasis G, Albers CA, Banks E, DePristo MA, et al. The variant call format and VCFtools. Bioinformatics. 2011;27(15):2156–8.
64. Liao Y, Peng Z, Fu S, Hua Y, Luo W, Liu R, et al. Elevated EBF2 in mouse but not pig drives the progressive brown fat lineage specification via chromatin activation. J Adv Res. 2024;76:327–44.

Publisher's Note